



A multi time-scale state-of-charge and state-of-health estimation framework using nonlinear predictive filter for lithium-ion battery pack with passive balance control

Yin Hua ^{a,*}, Andrea Cordoba-Arenas ^b, Nicholas Warner ^b, Giorgio Rizzoni ^b

^a National Engineering Laboratory for the Automotive Electronic Control Technology, Shanghai Jiao Tong University, 800 Dongchuan Rd., Shanghai 200240, China

^b Center for Automotive Research, The Ohio State University, 930 Kinnear Road, Columbus, OH 43212, USA



HIGHLIGHTS

- A multi time-scale SOC/SOH estimation framework for battery pack is presented.
- The battery pack is in series topology with passive balance control.
- The estimation framework is performed based on pack-level state definitions.
- Nonlinear predictive filter is used to provide accurate estimation results.
- UDDS profiles are used to validate the performance of the proposed framework.

ARTICLE INFO

Article history:

Received 26 October 2014

Received in revised form

14 January 2015

Accepted 18 January 2015

Available online 19 January 2015

Keywords:

State of charge

State of health

Lithium-ion battery pack

Electric vehicles

Nonlinear predictive filter

Passive balance control

ABSTRACT

With respect to cell-to-cell variation in battery packs for electric vehicles (EVs), the estimation of state of charge (SOC) and state of health (SOH) of battery systems remains a challenging problem that needs to be solved under the strict computational limitations of battery management system. This paper aims at proposing a stable and accurate SOC/SOH estimation framework for battery pack with multi-cells connected in series with passive balance control. First, the concepts of cell-level and pack-level state definitions, which clearly describe the relationship between the states of the battery cells and those of the battery pack, are introduced. Then a multi time-scale framework for estimating the SOC/SOH of pack is developed. Within the framework, the SOH values (slow dynamics) are estimated with long time interval, while the SOC (fast dynamics) is estimated in real-time. For the framework implementation, nonlinear predictive filter (NPF) is used as the estimation algorithm to provide accurate estimates of SOC and SOH. Finally, experiments are conducted on a battery pack under UDDS driving cycles to validate the performance of the proposed framework. The experimental validation indicates that the SOC and SOH of the battery pack can be accurately estimated using the proposed framework.

© 2015 Elsevier B.V. All rights reserved.

1. Introduction

With the development of electric vehicles (EVs) in recent years, the lithium-ion batteries, as the energy source for EVs, attract more and more attentions for its high energy and power density and long lifespan [1,2]. For an intelligent monitoring of the lithium-ion

battery, a battery management system (BMS) is required to accurately estimate the state of charge (SOC) and state of health (SOH) of the battery pack. The SOC is a crucial factor that indicates the residual capacity of battery system and helps predicting the remaining driving range of EVs [3]. Also, an accurate SOC estimation plays an important role in preventing the battery pack from over-charge and over-discharge which damage battery [4]. The SOH is another important aspect which should be estimated by the BMS [5,6], it is usually described by some battery parameters correlated with its aging such as resistance and capacity, indicating the ‘power fade’ and ‘capacity fade’ of battery pack, respectively.

* Corresponding author. Institute of Automotive Engineering, School of Mechanical Engineering, Shanghai Jiao Tong University, 800 Dongchuan Rd., Shanghai 200240, China.

E-mail address: hua.yin1986@163.com (Y. Hua).

For EV applications, in order to meet the high capacity requirement and provide the desired voltage, the battery pack usually consists of hundreds of cells, which are connected in series and parallel [7]. Many SOC estimation methods have been developed based on the assumption that all the cells in the pack behave equally, and therefore, the battery pack can be conveniently modeled as a unit cell with higher voltage and larger capacity. These approaches include current integration method [8,9], open circuit voltage method [10,11], black-box model based method [12,13] and model based filtering method [14–19]. Each method has its own advantages and disadvantages. The current integration method is simple to implement with a low computational effort, but the estimation accuracy will decrease due to the accumulative errors caused by current sensor noises. Therefore, this method is often corrected by open circuit voltage method. The black-box model based method usually uses a data-trained black-box model, such as neural networks [12] and support vector regression [13], to estimate the battery SOC. The estimation can be quite accurate with sufficient offline training data, but the computational effort is particularly high. The model based filtering method is usually performed on a state space battery model and is viewed as the most promising way to estimate battery SOC because of the high estimation accuracy and online state error correction capability. Many optimum state estimation approaches have been investigated for the model based filtering method, such as sliding mode observer [14], extend Kalman filter (EKF)[15], unscented Kalman Filter (UKF)[16], adaptive extended Kalman filter (AEKF) [17], adaptive unscented Kalman filter (AUKF)[18] and particle filter (PF) [19]. Most of them have achieved acceptable results according to the literature. In a similar fashion (i.e. using a unit cell model to represent the entire battery pack) some of these estimation approaches have been also used to estimate the SOH of battery pack by means of estimating the resistance and capacity, such as dual sliding mode observer [20] and dual extended Kalman filter [6,15].

However, in real world applications, in a battery pack there is some cell-to-cell variation due to manufacturing variability and inhomogeneous working environments (such as thermal imbalance) [21,22]. The cell-to-cell variation will become even larger as the cells age, which makes the unit cell model assumption unsuitable to represent battery pack. In addition to this, in a battery pack the SOC as well as the ability to store energy and deliver power, and therefore the system level SOC/SOH, highly depends on individual cell's performance, SOH, electrical topology and balance control [32]. For example, in a battery pack composed of cells in series with a passive balance control, the 'weakest cell' will firstly reach fully discharged state during the discharge operation, limiting the discharge capacity of the entire pack. A similar situation will happen during charge operation. Therefore, the 'pack states' as defined in the unit cell model do not accurately describe the battery pack SOC/SOH. As a result, an estimation based on unit cell model will be inaccurate for real world applications.

Different methods have been proposed to take into account the variability of cells in the battery SOC/SOH estimation. Plett [23] proposed a bar-delta filtering method based on SPKF to estimate the SOC and SOH values of every cell in the pack. Dai et al. [24] introduced a dual time-scale extended Kalman filtering (EKF) method to estimate the pack 'average SOC' first, and then they incorporate the performance divergences between the 'averaged cell' and each individual cell to generate the SOC estimations for all cells. Both Plett and Dai et al. use the bar-delta filter concept to reduce the computational effort of estimating the states of each individual cell in the pack. However there are still hundreds of delta filters running in the battery management system and therefore the computational effort is still significant. Kim et al. [25] proposed a stable SOC estimation method using EKF based on a screening

process for improved voltage/SOC balancing of a lithium-ion series battery pack. Xiong et al. [26] also used a similar approach based on cell screening process but with AEKF to improve the estimation accuracy. Both Kim et al. and Xiong et al. preprocess the cells with a carefully defined cell screening process to make up a battery pack with good consistence. But in practical, it is almost unrealistic to get the parameters of every cell when making up the pack in mass production, thus the cell screening process is difficult to implement. Roscher et al. [27] introduced a reliable state estimation of multi-cells lithium-ion battery systems, by which cell impedance and SOC variations could be detected precisely. But how to determine the tunable correction gain was not discussed in this paper. Zheng et al. [28] introduced a cell state-of-charge inconsistency estimation for LiFePO₄ battery pack using mean-difference model, and SOC differences is determined with estimated OCV differences using SOC-difference/OCV-difference curve. However, to implement this method, hundreds of total least squares methods are needed to obtain the OCV differences when applying it to the battery pack in EVs, which makes its application unrealistic due to the high computational effort. Zhong et al. [29] proposed an estimation method for the battery pack state of charge based on in-pack cells uniformity analysis, the relationship between the parameters of the pack and those of in-pack cells under different balance control strategies is established in order to estimate the pack SOC, and then the pack SOC estimation can be converted into SOC estimation for the weakest cells. However, how to perform an online identification of the weakest cells is not discussed in this paper. Liu et al. [30] introduced a SOC estimation method based on minimal cell terminal voltage of the battery pack. But with the fact that the cell with minimal terminal voltage is not always the cell with the lowest capacity, the estimation can be inaccurate in some special situations.

In this paper, in order to accurately estimate the SOC and SOH of battery pack with a low computational effort, a multi time-scale nonlinear predictive filter (NPF) estimation framework is proposed. First, both cell-level and pack-level SOC/SOH definitions are presented based on series connected battery pack with passive balance control. For a battery system with these characteristics, the SOC and capacity of battery pack can be represented by the 'weakest in-pack cell' with minimum capacity, and the pack resistance is represented by the sum of all the in-pack cells' resistances. Then the multi time-scale estimation framework is presented. The framework separately evaluates the pack SOH estimate with an 'offline' long time-scale and the pack SOC estimate with a real-time implementation with respect to the multi time-scale nature of battery systems. In the long time-scale estimation part, the resistances and capacities of all the cells in the pack are estimated with a long time interval, and the SOH of the pack are obtained based on the pack-level definitions. After that a cell screening process is implemented to select the 'weakest cell' based on the estimation results of cells' capacities. In the real-time implementation part, based on the cell screening results, the estimation of pack SOC is reduced into the SOC estimation of the 'weakest cell'. With respect to estimate every cell's SOC, the proposed framework only needs to estimate one cell which greatly reduces the computational effort. Compared to the above mentioned estimation methods using unit cell model, the proposed method has better estimation accuracy since it takes into account the cell-to-cell variation and the estimation is implemented based on pack-level SOC/SOH definitions. In comparison with the bar-delta filtering method, the proposed approach requires a lower computational effort, due to the fact that it just requires estimating the SOC of the weakest cell.

During the past years, the Extended Kalman filter (EKF) has been widely accepted as the state estimation algorithm for batteries. In

EKF, the process noise is assumed to be zero mean Gaussian process and a priori knowledge of the covariance of the process noise is required. However, in actual practice the determination of the process noise covariance can be very difficult due to the nonlinearities of battery systems. In fact, the zero-mean Gaussian process noise assumption has not been proved when using equivalent circuit model to represent the battery system. In general, an inaccurate process noise covariance will decrease the estimation accuracy of EKF. In this context, the proposed NPF approach has significant advantages compared to EKF including: (i) the process noise is assumed unknown and is estimated as part of the solution, (ii) the process noise may take any distribution form (i.e. non-zero mean non-Gaussian process). Therefore, in this work, the NPF [31] is applied as model based state estimation algorithm in the multi-time-scale estimation framework.

The rest of the paper is organized as follows. In Section 2, the cell-level and pack-level definitions for battery systems are introduced. In Section 3, a description of the proposed SOC/SOH estimation framework for battery packs is presented. In Section 4, an experimental plan is conducted on a battery pack, and the estimation results are analyzed and discussed to verify the proposed method. Finally, the conclusions are provided in Section 5.

2. Advanced battery systems

This section presents general aspects of battery systems as well as the notations and definitions used through this work.

2.1. Cell-level definitions of battery states

The nominal capacity of a single cell is defined as the amount of charge stored within the cell between the specific voltage limits defined by the cell manufacturer. The nominal capacity of a single battery cell is therefore given by the total discharge capacity defined as the total ampere-hour throughput that can be drawn from the cell starting from the upper-limit voltage (fully charged) to lower-limit voltage (fully discharged) with a current rate of 1C at room temperature (25 °C).

As illustrated in Fig. 1, the SOC of a single cell is the ratio of the remaining capacity to the nominal capacity of the cell, where the remaining capacity is the number of ampere-hours that can be drawn from the cell before it is fully discharged [8]. Operationally, the SOC of a single battery cell is given by:

$$SOC(t) = SOC(0) + \int_0^t \frac{\eta I_L(t) dt}{C} \quad (1)$$

where $SOC(0)$ represents the battery SOC at initial condition, $SOC(t)$ represents the SOC at time t , η represents the coulombic efficiency

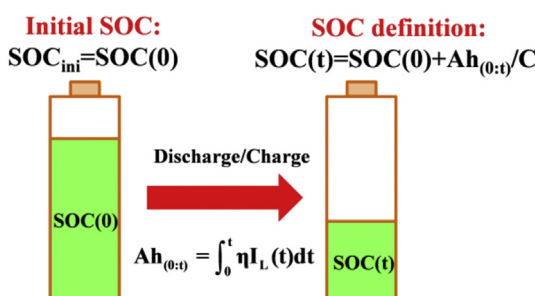


Fig. 1. Schematic diagram of SOC definition for a single battery cell.

which is the function of temperature and cell current, $I_L(t)$ is instantaneous cell current (assumed to be positive for charge and negative for discharge), and C is the nominal capacity of the cell.

Generally, battery-aging manifest itself in a reduction in the ability to store energy and deliver power, performance metrics correlated with loss in capacity and increase in internal resistance. Among the micro-mechanisms of lithium-ion battery aging we cite active particle loss and metal sediment or SEI film accumulation. A review of today's knowledge on the mechanics of aging in lithium-ion batteries can be found in Ref. [40]. These physical-chemical mechanisms are enhanced by stress factors such as Temperature, SOC, depth of discharge (DOD) and C-rate [40,41]. The SOH of a battery cell, which is used to describe the cell's physical condition, is commonly characterized by a cell parameter that is correlated with its aging. Depending on the application, the SOH of a battery cell may be characterized by loss in capacity, increase in internal resistance, or a combination of both [41,42]. In this work, we refer as capacity state of health (SOH_C) to the figure of merit that is correlated with the battery's ability to store energy; and refer as power state of health (SOH_R) to the figure of merit that is correlated with the battery's ability to deliver power.

We adopt the definition of SOH_C for a single cell as the ratio of the present cell available capacity $C_{present}$ to the nominal cell's capacity C_0 :

$$SOH_C = \frac{C_{present}}{C_0} \quad (2)$$

For a fresh cell, $SOH_C = 1$ and slowly decreases with aging. For automotive applications, from a capacity stand point; the cell end-of-life (EOL) is reached when SOH_C reaches 0.8 (i.e. 20% in capacity loss).

Similarly, we adopt the definition of SOH_R for a single cell as the present cell internal resistance $R_{present}$ to the nominal cell's resistance R_0 :

$$SOH_R = \frac{R_{present}}{R_0} \quad (3)$$

For a fresh cell, $SOH_R = 1$ and slowly increases with aging. For automotive applications, from a power performance stand point; the cell end-of-life (EOL) is reached when SOH_R is larger than the pre-defined threshold. Different definitions of the thresholds for SOH_R have been defined in the literature in Refs. [43–45], therefore there is not yet a widely established threshold.

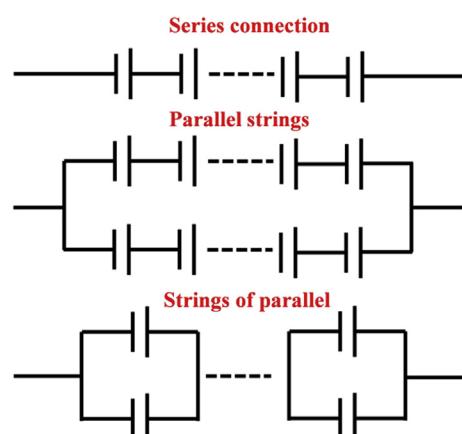


Fig. 2. Battery electrical topologies: (high) Series connection, (mid) Parallel strings of cells, (low) Strings of parallel cells.

2.2. Pack-level definitions for battery states

A battery pack in electrified vehicle applications is made up of series and parallel combinations of individual cells. Cells are connected in parallel to satisfy high capacity requirements and in series to provide the desired system voltage. Fig. 2 shows the different types of electrical topologies: series connection, parallel strings of cells and strings of parallel cells [32]. In a pack, cell parameters such as battery capacity and internal resistance, varies from cell-to-cell due to manufacturing variability, aging, and different operational conditions such as temperature gradient within the pack. Cell-to-cell variation in voltage, capacity, internal resistance, and SOC negatively affect the available energy of a battery system, reducing the performance and lifespan of battery pack. Therefore, different balance control methods are used by a battery management system (BMS) to deal with the cell-to-cell variation and therefore to improve battery system performance; these balance control methods can be classified into: passive and active balance [33]. Compared to the active balance approaches, the passive balance control is the most commonly used in commercial EVs due to its low cost and low complexity. By applying different balance control methods to a battery system, the SOC of individual cells in the pack as well as the pack available capacity changed accordingly, so the influence of the balance control method needs to be taken into account when estimating the SOC/SOH of the battery pack.

In a battery pack the ability to store energy and deliver power, and therefore the system level SOH, highly depends on individual cell's performance and SOH, electrical topology, and balance control [32]. In this work, we specifically focus our attention on the state estimation problem for a battery pack composed of cells connected in series configuration with a passive balance control. The SOC, capacity and resistance of the cells in the same battery pack with series connection are denoted by SOC_i, C_i, R_i , respectively, where $i \in [1, \dots, n]$. Extending the concept of the capacity definition for an individual cell into pack level definition, the pack capacity is given by the total ampere-hours drawn from the fully charged cell in the battery pack until one of the cells in the pack is fully discharged. It can be represented by the sum of the minimum cell capacity that can be charged and the minimum remaining cell capacity that can be discharged [34], as given in Eq. (4):

$$C_{\text{pack}} = \min_{1 \leq i \leq n} (SOC_i C_i) + \min_{1 \leq j \leq n} ((1 - SOC_j) C_j) \quad (4)$$

where C_{pack} is battery pack capacity, $\min_{1 \leq i \leq n} (SOC_i C_i)$ represents the minimum remaining capacity among the cells and $\min_{1 \leq j \leq n} ((1 - SOC_j) C_j)$ represents minimum chargeable capacity among the cells. Therefore, the SOC definition for battery pack can be defined by the ratio of the minimum remaining capacity to the

pack capacity, given as follow:

$$SOC_{\text{pack}} = \frac{\min_{1 \leq i \leq n} (SOC_i C_i)}{C_{\text{pack}}} \quad (5)$$

Specifically for a battery pack with passive balance control, the cells in the same pack will be balanced to the same SOC at initial condition, and the cell with minimum capacity will first reach the fully discharged state (i.e. reach lower-limit voltage). A schematic diagram illustrates the discharge process of battery pack with passive balance control is given in Fig. 3, a pack consists of three cells with the capacity of 4.4Ah, 4.2Ah and 4.0Ah is taken as an example. The initial condition for three cells is set to the fully charged state with 100% SOC, when one of cells (No.3) reaches the lower-limit voltage, the battery pack is considered as fully discharged, the capacity and SOC of cell.3 represents the pack capacity and pack SOC. Therefore, the definitions of capacity and SOC for the battery pack with passive balance control can be given as follows:

$$C_{\text{pack}} = \min_{1 \leq i \leq n} (C_i) = C_{\text{min_cell}} \quad (6)$$

$$SOC_{\text{pack}} = SOC_{\text{min_cell}} = SOC(0) + \int_0^t \frac{\eta I_L(t) dt}{C_{\text{min_cell}}} \quad (7)$$

where $C_{\text{min_cell}}$ and $SOC_{\text{min_cell}}$ are the minimum capacity and minimum SOC among the cells, respectively.

Since the cells are connected in series, the resistance of the battery pack is the sum of the cells' resistances, given as follow:

$$R_{\text{pack}} = \sum_{i=1}^n R_i \quad (8)$$

A detailed methodology to assess the SOH of a battery pack from knowledge of individual cells SOH, electrical topology and balance control approach is presented in our previous work [32]. The capacity SOH of a battery pack is correlated with the pack capacity, for a pack composed of cells in series with passive balance, it is defined as:

$$SOH_{C,\text{pack}} = \min_{1 \leq i \leq n} (SOH_{C,i}) \quad (9)$$

where $SOH_{C,\text{pack}}$ is the pack capacity state of health, and $SOH_{C,i}$ is the capacity state-of-health for a cell index number i . The pack power capability is restricted by the lower voltage limit of each cell among the battery pack. The cell with largest resistance will first reach the lower voltage limit and thus the pack power SOH is determined by the cell with largest resistance. The power SOH for a pack

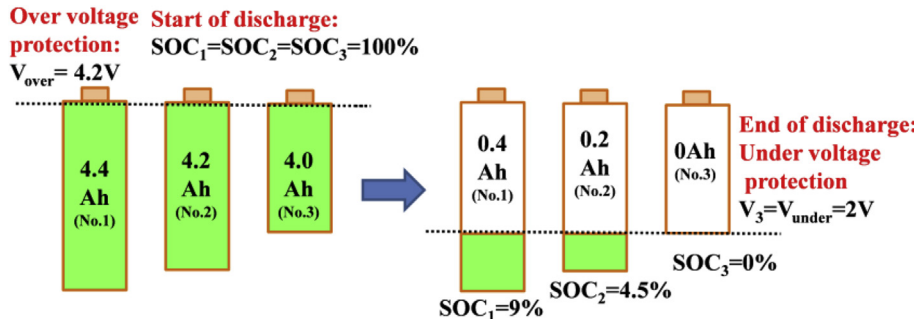


Fig. 3. Discharge of battery pack with passive balance control.

composed of cells in series with passive balance is defined as:

$$SOH_{R,pack} = \max_{1 \leq i \leq n} (SOH_{R,i}) \quad (10)$$

where $SOH_{R,pack}$ is the pack power state of health, and $SOH_{R,i}$ is the power state-of-health for a cell index number i .

With these definitions in mind and for simplicity of the discussion, we cast the SOC/SOH estimation problem into a SOC, capacity and internal resistance estimation problem.

3. Proposed SOC and SOH estimation strategy

In this section, a multi time-scale framework for estimating the SOC/SOH of advanced battery systems with series topology under passive balance is proposed and discussed. According to the definitions for battery pack in section 2, in order to get the states of battery pack, the cell-level information of the battery pack needs to be known. However, to separately estimate the states of every battery cell at every time step will cause extremely high computational effort, and thus it is not practical for real-world applications. Therefore we propose a framework that exploits the multi time-scale nature of battery systems, with respect to the fact that the battery SOH has much slower dynamic compare to the battery SOC. The proposed framework is such that the SOC of the battery pack is estimated ‘on-line’ in real-time while the SOH of the battery pack is estimated ‘off-line’ (e.g. when the EV is parked) using a long time interval (e.g. several weeks once). In this context the SOC/SOH estimation framework consist of two main parts. In one part, an ‘off-line’ cell screening process is performed to determine the weakest cell with the lowest capacity and therefore the battery pack SOH based on the daily driving profiles (current and voltage of one day’s driving profiles) which may be stored in the BMS. In the other part, once the weakest cell has been identified, the SOC of the pack (determined by the SOC of the weakest cell in the pack) is estimated online. A schematic of the multi time-scale estimation framework is presented in Fig. 4.

This subsection is organized as follows; first, equivalent circuit model (ECM) is developed to model the battery cell/pack performance. Then a dual nonlinear predictive filter (DNPF) is used for cell-level estimation, including battery SOC, resistance and capacity. Finally, based on the cell-level estimation, a multi time-scale estimation framework is proposed to extend the cell-level estimation approach into the pack-level.

3.1. Battery model

To implement the model based estimation methodology, a battery model is needed to characterize the electrochemical properties of battery cell, such as ohmic resistance, charge transfer and diffusion phenomenon. Different battery modeling approaches

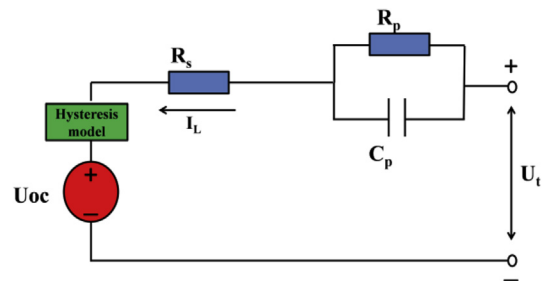


Fig. 5. Schematic diagram of the first-order ECM for a single cell.

have been proposed to predict battery performance. In particular, electrochemical models [35] and equivalent circuit models (ECMs) [36] are the most commonly used approaches to model traction battery systems. Electrochemical models make use of first principles and are described by partial differential equations (PDEs). Due to their mathematical complexity, they are not very suitable in solving real-time state estimation problems. ECMS try to capture the battery input–output dynamics through electrical circuit elements. The construction of the equivalent circuit models can be obtained by electrochemical impedance spectroscopy (EIS), or by time domain identification techniques. ECMS represent an excellent compromise between accuracy and complexity which makes them suitable for real-time applications. Moreover, the control-oriented nature of ECMS makes them suitable for online model based SOC/SOH estimation. Therefore a first-order ECM is used in this work for the purpose of modeling each individual cell in the battery pack.

To model the performance of each individual cell, the circuit is composed of an open-circuit voltage source, a series resistance, an RC network and a hysteresis voltage source, see Fig. 5. The dynamic equation that describes the voltage across the RC network is given by:

$$\dot{U}_p(t) = -(R_p C_p)^{-1} U_p(t) + C_p^{-1} I_L(t) \quad (11)$$

where R_p is the equivalent polarization resistance, C_p is the equivalent polarization capacitance, U_p is the voltage on C_p , and I_L is the input current. The dynamic equation describes the hysteresis voltage is given as follow [17]:

$$\dot{h}(t) = -\left|\frac{\eta I_L(t)\gamma}{C}\right| h(t) + \left|\frac{\eta I_L(t)\gamma}{C}\right| M(SOC(t), \dot{SOC}(t)) \quad (12)$$

where h represents the hysteresis voltage, γ can be considered as a hysteresis transition factor (i.e. how fast the hysteresis occurs) and M is the magnitude of hysteresis voltage which is the function of SOC and current. The terminal voltage is given by:

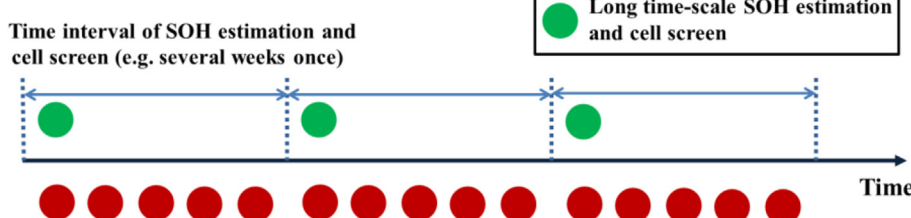


Fig. 4. Schematic diagram of multi time-scale estimation.

$$U_t(t) = U_{oc}(t) + U_p(t) + I_L(t)R_s + h_k(t) \quad (13)$$

where U_t is the terminal voltage, R_s is the series ohmic resistance, the open circuit voltage U_{oc} is the function of SOC which is described by Eq (14):

$$U_{oc}(t) = Spline(SOC(t)) \quad (14)$$

Here a spline function is used to fit the SOC-OCV curve.

To model the battery pack, which is composed of several cells connected in series configuration, a series of first order ECMs is adopted, see Fig. 6.

3.2. Nonlinear predictive filter description

Nonlinear predictive filter (NPF) is a model based optimum state estimation method implemented on nonlinear continuous-discrete time system [31]. The advantage of NPF compared to most filters is that, in NPF the process noise can take any form (i.e. non-zero mean non-Gaussian process) and the process noise is estimated as part of the solution. In the continuous-discrete time system, the state equation consists of a system dynamic part and model error part, given as follows:

$$\text{State equation : } \dot{x}(t) = f[x(t), t] + g(t)d(t) \quad (15)$$

where $x(t)$ is the state vector, f is the function describes the system dynamic, $g(t)$ is the model error distribution matrix, $d(t)$ is the model error vector which mainly represents the process noises.

The measurement equation for the nonlinear continuous-discrete time system is given by:

$$\text{Measurement equation : } y(t_k) = h[x(t_k), t_k] + v(t_k) \quad (16)$$

where $y(t_k)$ is the system output sampled at time step k , h is the measurement function, v is the measurement noise vector which is assumed to be an independent Gaussian white noise with zero mean and

$$E[v(t_k)] = 0, E[v(t_k)v(t_k)^T] = R\delta_{kk} \quad (17)$$

In order to obtain the optimal estimation of $x(t)$ in NPF, $d(t)$ needs to be accurately estimated at every time step, the estimation of $d(t)$ is achieved by solving a cost function. The cost function to be minimized in NPF is developed based on minimum model error (MME) principle [37], which consists of two parts: a weighted sum square of the measurement-minus-estimate residuals and a weighted sum square of the model error correction term, as given in Eq. (18):

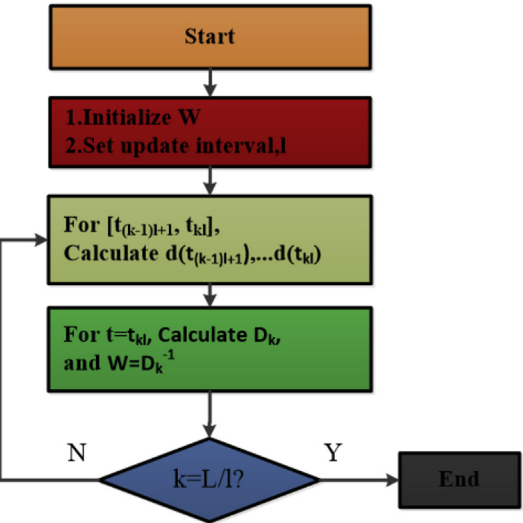


Fig. 7. Workflow for updating weighting matrix.

$$\begin{aligned} J[d(t)] = & 0.5[y(t + \Delta t) - \hat{y}(t + \Delta t)]^T R^{-1} [y(t + \Delta t) - \hat{y}(t + \Delta t)] \\ & + 0.5d(t)^T W d(t) \end{aligned} \quad (18)$$

where $y(t) = y(t_k), y(t + \Delta t) = y(t_{k+1})$, Δt is the sampling interval, W is a positive semi-definite weighting matrix. $y(t)$ and $\hat{y}(t)$ are the measured output and estimated output, respectively.

The estimated output $\hat{y}(t + \Delta t)$ is approximated by the first order Taylor expansion, given by:

$$\begin{aligned} \hat{y}(t + \Delta t) = & \hat{y}(t) + \Delta t \dot{\hat{y}}(t) + 0.5\Delta t^2 \ddot{\hat{y}}(t) + \dots \approx \hat{y}(t) + Z(\hat{x}(t), \Delta t) \\ & + \Lambda(\Delta t)S(\hat{x}(t))d(t) \end{aligned} \quad (19)$$

where $S(\hat{x}(t_k)), Z(\hat{x}(t_k), \Delta t), \Lambda(\Delta t)$ are intermediate matrices, the solutions of $S(\hat{x}(t_k)), Z(\hat{x}(t_k), \Delta t), \Lambda(\Delta t)$ are defined using the knowledge of Lie derivation, given by:

$$S(\hat{x}(t)) = \begin{bmatrix} L_{g_1}L_f^{r_1-1}h_1(\hat{x}(t)) & \cdots & L_{g_l}L_f^{r_1-1}h_1(\hat{x}(t)) \\ \vdots & \ddots & \vdots \\ L_{g_1}L_f^{r_m-1}h_m(\hat{x}(t)) & \cdots & L_{g_l}L_f^{r_m-1}h_m(\hat{x}(t)) \end{bmatrix} \quad (20)$$

$$\Lambda(\Delta t) = \begin{bmatrix} \lambda_{11} & \cdots & 0 \\ \vdots & \lambda_{ii} & \vdots \\ 0 & \cdots & \lambda_{mm} \end{bmatrix}, \lambda_{ii} = \frac{\Delta t^{r_i}}{r_i!}, i = 1, 2, \dots, m \quad (21)$$

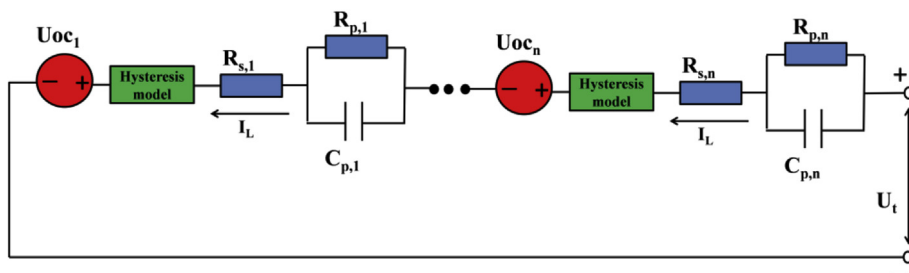


Fig. 6. Schematic Diagram of ECM for series connected battery pack.

$$Z_i(\hat{x}(t), \Delta t) = \sum_{a=1}^{r_i} \frac{\Delta t^a}{a!} L_f^a h_i(\hat{x}(t)), i = 1, 2, \dots, m \quad (22) \quad L_g L_f^{n_i} h_i(\hat{x}(t)) = 0 (i = 1, 2, \dots, m; j = 1, 2, \dots, l, n_i < r_i - 1) \quad (26)$$

where $L_g L_f^{r_i-1} h_i(\hat{x}(t))$ is the Lie derivation, defined by:

$$L_f^0 h_i(\hat{x}(t)) = h_i(\hat{x}(t)) \quad (23)$$

$$L_f^n h_i(\hat{x}(t)) = \frac{\partial L_f^{n-1} h_i(\hat{x}(t))}{\partial \hat{x}} f[\hat{x}(t), t] \quad (24)$$

$$L_g L_f^n h_i(\hat{x}(t)) = \frac{\partial L_f^n h_i(\hat{x}(t))}{\partial \hat{x}} g_j(t) \quad (25)$$

The index r_i is the relative degree, which satisfies the following equations:

$$L_g L_f^{r_i-1} h_i(\hat{x}(t)) \neq 0 (i = 1, 2, \dots, m; j = 1, 2, \dots, l) \quad (27)$$

Then, the solution of $d(t)$ is can be derived by minimizing the cost function $J[d(t)]$, given by:

$$d(t) = - \left\{ [A(\Delta t)S(\hat{x}(t))]^T R^{-1} A(\Delta t)S(\hat{x}(t)) + W \right\}^{-1} \times [A(\Delta t)S(\hat{x}(t))]^T R^{-1} [Z(\hat{x}(t), \Delta t) + \hat{y}(t) - y(t + \Delta t)] \quad (28)$$

where the weight matrix W is given by the inverse of the model error's covariance matrix D , given as follows:

Table 1
Summary of nonlinear predictive filter.

Nonlinear the continuous-discrete time model^a

$$\dot{x}(t) = f[x(t), t] + g(t)d(t)$$

$$y(t_k) = h[x(t_k), t_k] + v(t_k)$$

Definitions

$$S(\hat{x}(t)) = \begin{bmatrix} L_{g_1} L_f^{r_1-1} h_1(\hat{x}(t)) & \dots & L_{g_1} L_f^{r_1-1} h_1(\hat{x}(t)) \\ \vdots & \ddots & \vdots \\ L_{g_m} L_f^{r_m-1} h_m(\hat{x}(t)) & \dots & L_{g_m} L_f^{r_m-1} h_m(\hat{x}(t)) \end{bmatrix}$$

$$\Lambda(\Delta t) = \begin{bmatrix} \lambda_{11} & \dots & 0 \\ \vdots & \lambda_{ii} & \vdots \\ 0 & \dots & \lambda_{mm} \end{bmatrix}, \lambda_{ii} = \frac{\Delta t^{r_i}}{r_i!}, i = 1, 2, \dots, m$$

$$Z_i(\hat{x}(t), \Delta t) = \sum_{a=1}^{r_i} \frac{\Delta t^a}{a!} L_f^a h_i(\hat{x}(t)), i = 1, 2, \dots, m$$

Initialization

$$\text{For } k = 0, \text{ set } \hat{x}(t_0) = E[x(t_0)]$$

$$W = E[(d(t_0) - E[d(t_0)])(d(t_0) - E[d(t_0)])^T]^{-1}$$

Set weighting matrix update time interval: $l = L/r$

Computation

For $k = 1, 2, \dots$ compute

Estimate system output: $\hat{y}(t_k) = h[\hat{x}(t_k)]$

$$\begin{aligned} d(t_k) &= -\{[\Lambda(\Delta t)S(\hat{x}(t_k))]^T R^{-1} \Lambda(\Delta t)S(\hat{x}(t_k)) + W\}^{-1} \\ &\times [\Lambda(\Delta t)S(\hat{x}(t_k))]^T R^{-1} [Z(\hat{x}(t_k), \Delta t) + \hat{y}(t_k) - y(t_{k+1})] \end{aligned}$$

State estimate update to $\hat{x}(t_{k+1})$ by state equation: $\dot{\hat{x}}(t) = f[\hat{x}(t), t] + g(t)d(t)$

For $k = nl, 1 \leq n \leq r$, compute

Covariance for $[d(t_{(k-1)l+1}), \dots, d(t_{kl})]$: $D_k = \text{Cov}[d(t)], t \in [t_{(k-1)l+1} : t_{kl}]$

Update weighting matrix: $W = D_k^{-1}$

^a v is an independent, zero-mean, Gaussian noise process with covariance R .

$$W = D^{-1} = \text{Cov}[d(t)]^{-1} = E[(d(t) - E[d(t)])(d(t) - E[d(t)])^T]^{-1} \quad (29)$$

Assume that $d(t)$ is a stationary ergodic random process, then W can be iteratively calculated with certain time interval, the workflow for calculating W is shown in Fig. 7, and the detail process is listed as follows:

- Step.1: Initialization: $W = E[(d(t_0) - E[d(t_0)])(d(t_0) - E[d(t_0)])^T]^{-1}$, for the total time length L , the time interval for updating W is selected as $l = L/r$, where r is the total iterations.
- Step.2: For $t \in [t_{(k-1)+1}: t_k]$: estimate the model error $d(t)$ for $[t_{(k-1)+1}: t_k]$, and get the model error sequence $[d(t_{(k-1)+1}, \dots, d(t_k)]$.
- Step.3: For $t = t_k$, update weighting matrix: $W = D_k^{-1}$, D_k is the covariance for $[d(t_{(k-1)+1}, \dots, d(t_k)]$.
- Step.4: If $k < L/l$, return to step.2.

Based on the previous discussion, after $d(t_k)$ is estimated, the state estimation can be propagated from $x(t_k)$ to $x(t_{k+1})$ by approximated discretization of the state equation for time t_k . The summary of the nonlinear predictive filter is given in Table 1.

In order to use the NPF for a battery management system, a battery model in continuous-discrete time form is needed. Taking as an example the application of NPF to estimate the battery SOC, the continuous state equation used in NPF is given by:

$$\begin{aligned} \text{State equation : } \dot{x}(t) &= \begin{pmatrix} \dot{\text{SOC}}(t) \\ \dot{U}_p(t) \\ \dot{h}(t) \end{pmatrix} \\ &= \begin{pmatrix} 0 \cdot \text{SOC}(t) + \frac{I_L(t)}{C} \\ -(R_p C_p)^{-1} U_p(t) + C_p^{-1} I_L(t) \\ -\left| \frac{\eta I_L(t) \gamma}{C} \right| h(t) + \left| \frac{\eta I_L(t) \gamma}{C} \right| M \end{pmatrix} + g \begin{pmatrix} d_1(t) \\ d_2(t) \\ d_3(t) \end{pmatrix} \end{aligned} \quad (30)$$

where SOC, U_p and h are chosen as state variables, $d_1(t), d_2(t), d_3(t)$

are the model errors for these three states. g is the model error distribution matrix which is assigned with an identity matrix. The discrete measurement equation is given by:

$$\begin{aligned} \text{Measurement equation : } y(t_k) &= U_t(t_k) \\ &= U_{oc}[\text{SOC}(t_k)] + U_p(t_k) + I_L(t_k) R_s \\ &\quad + h_k(t_k) + v(t_k) \end{aligned} \quad (31)$$

where the battery terminal voltage U_t is chosen as the system output variable, v represents the measurement noise which is an independent, zero-mean, Gaussian noise process with covariance R . Fig. 8 shows a control oriented block diagram of the NPF method for battery state estimation.

3.3. Dual nonlinear predictive filter for cell-level estimation

Similar to the idea of dual Extended Kalman filter for battery estimation [15], a dual nonlinear predictive filter (DNPF) estimation approach is proposed in this work for the battery SOC and SOH estimation. The DNPF approach includes a state filter and a weight filter.

For the state filter in DNPF, the battery dynamic model is slightly modified to explicitly include the parameters, given by:

$$\text{State equation : } \dot{x}(t) = f[x(t), t, \theta(t)] + g_x(t)d_x(t) \quad (32)$$

$$\text{Measurement equation : } y(t_k) = h[x(t_k), t_k, \theta_k] + v(t_k) \quad (33)$$

where $x(t)$ is the state vector, θ is the time-varying parameters, $g_x(t)$ is the model error distribution matrix for state filter which is assigned with an identity matrix, $d_x(t)$ is the model error vector for state filter.

For the weight filter in DNPF, the battery's parameters need to be estimated are treated as the state variables, given by:

$$\begin{aligned} \text{State equation : } \dot{\theta}(t) &= r[x(t), t, \theta(t)] + g_\theta(t)d_\theta(t) \\ &= 0 \cdot \theta + g_\theta(t)d_\theta(t) \end{aligned} \quad (34)$$

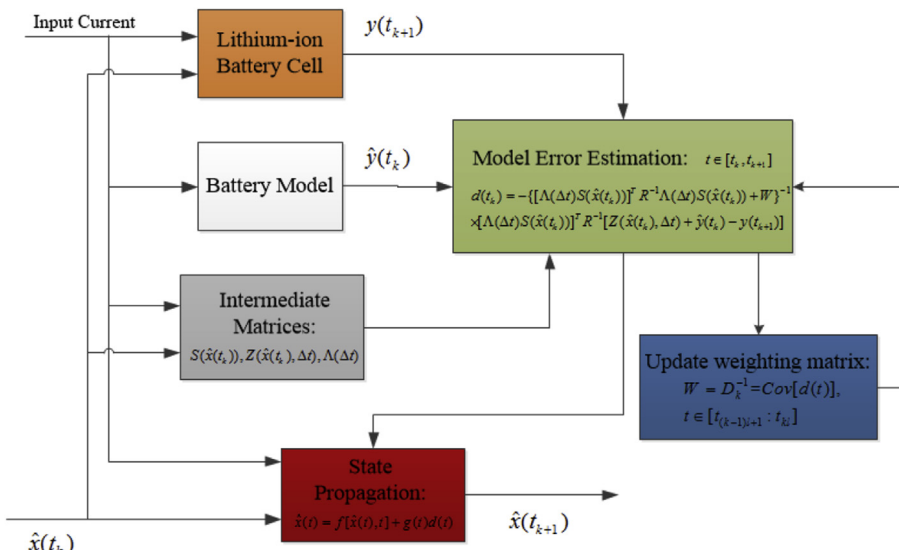


Fig. 8. Control oriented block diagram of NPF method for battery state estimation.

$$\text{Measurement equation : } p(t_k) = q[x(t_k), t_k, \theta(t_k)] + \omega(t_k) \quad (35)$$

where $\theta(t)$ is state variables in weight filter, $g_\theta(t)$ is the model error distribution matrix for weight filter which is assigned with an identity matrix, ω is an independent, zero-mean, Gaussian noise process with covariance Q . Since the parameters to be estimated change very slowly, the state equation in weight filter states that the parameters are essentially constant with ‘zero’ dynamics, the

tracking of parameters change is mainly fulfilled by the model error part. The summary of dual nonlinear predictive filter is given in **Table 2**.

To apply the DNPF method to battery system, suitable battery model with continuous-discrete time form is needed for both state filter and weight filter. In the state filter, we take the battery SOC, battery resistance, polarization voltage and hysteresis voltage as the state variables, the state and measurement equations for state filter are given as follows:

Table 2
Summary of dual nonlinear predictive filter.

Nonlinear the continuous-discrete time model^a

$$\dot{x}(t) = f[x(t), t, \theta(t)] + g_x(t)d_x(t), \quad \dot{\theta}(t) = r[x(t), t, \theta(t)] + g_\theta(t)d_\theta(t)$$

$$y(t_k) = h[x(t_k), t_k, \theta_k] + v(t_k), \quad p(t_k) = q[x(t_k), t_k, \theta_k] + \omega(t_k)$$

Definitions

$$S_x(\hat{x}(t)) = \begin{bmatrix} L_{g_{x1}} L_f^{r_1-1} h_1(\hat{x}(t)) & \dots & L_{g_{x,r}} L_f^{r_1-1} h_r(\hat{x}(t)) \\ \vdots & \ddots & \vdots \\ L_{g_{x1}} L_f^{r_m-1} h_m(\hat{x}(t)) & \dots & L_{g_{x,r}} L_f^{r_m-1} h_m(\hat{x}(t)) \end{bmatrix}, \quad S_\theta(\hat{\theta}(t)) = \begin{bmatrix} L_{g_{\theta1}} L_r^{r_1-1} q_1(\hat{\theta}(t)) & \dots & L_{g_{\theta,r}} L_r^{r_1-1} q_1(\hat{\theta}(t)) \\ \vdots & \ddots & \vdots \\ L_{g_{\theta1}} L_r^{r_m-1} q_m(\hat{\theta}(t)) & \dots & L_{g_{\theta,r}} L_r^{r_m-1} q_m(\hat{\theta}(t)) \end{bmatrix}$$

$$\Lambda_x(\Delta t) = \begin{bmatrix} \lambda_{11} & \dots & 0 \\ \vdots & \lambda_{ii} & \vdots \\ 0 & \dots & \lambda_{mm} \end{bmatrix}, \quad \lambda_{ii} = \frac{\Delta t^{r_i}}{r_i!}, \quad i=1, 2, \dots, m \quad , \quad \Lambda_\theta(\Delta t) = \begin{bmatrix} \lambda_{11} & \dots & 0 \\ \vdots & \lambda_{ii} & \vdots \\ 0 & \dots & \lambda_{mm} \end{bmatrix}, \quad \lambda_{ii} = \frac{\Delta t^{r_i}}{r_i!}, \quad i=1, 2, \dots, m$$

$$Z_{x,i}(\hat{x}(t), \Delta t) = \sum_{a=1}^{r_i} \frac{\Delta t^a}{a!} L_f^a h_i(\hat{x}(t)), \quad i=1, 2, \dots, m \quad , \quad Z_{\theta,i}(\hat{\theta}(t), \Delta t) = \sum_{a=1}^{r_i} \frac{\Delta t^a}{a!} L_r^a q_i(\hat{\theta}(t)), \quad i=1, 2, \dots, m$$

Initialization

$$\text{For } k=0, \text{ set } \hat{x}(t_0) = E[x(t_0)], \quad \hat{\theta}(t_0) = E[\theta(t_0)]$$

$$W_x = E[(d_x(t_0) - E[d_x(t_0)])(d_x(t_0) - E[d_x(t_0)])^T]^{-1}, \quad W_\theta = E[(d_\theta(t_0) - E[d_\theta(t_0)])(d_\theta(t_0) - E[d_\theta(t_0)])^T]^{-1}$$

Set weighting matrix update time interval: $l=L/r$

Computation

For $k=1, 2, \dots$ compute

$$\text{Estimate output for state filter: } \hat{y}(t_k) = h[\hat{x}(t_k), \theta(t_k)]$$

$$\begin{aligned} \text{Estimate model error for state filter: } d_x(t_k) &= -\{[\Lambda_x(\Delta t)S_x(\hat{x}(t_k))]^T R^{-1} \Lambda_x(\Delta t)S_x(\hat{x}(t_k)) + W_x\}^{-1} \\ &\times [\Lambda_x(\Delta t)S_x(\hat{x}(t_k))]^T R^{-1} [Z_x(\hat{x}(t_k), \Delta t) + \hat{y}(t_k) - y(t_{k+1})] \end{aligned}$$

$$\text{State filter update to } \hat{x}(t_{k+1}) \text{ by state equation: } \dot{\hat{x}}(t) = f[\hat{x}(t), t, (t_k)] + g_x(t)d_x(t)$$

$$\text{Estimate output for weight filter: } \hat{p}(t_k) = q[\hat{x}(t_{k+1}), \hat{\theta}(t_k)]$$

$$\begin{aligned} \text{Estimate model error for weight filter: } d_\theta(t_k) &= -\{[\Lambda_\theta(\Delta t)S_\theta(\hat{\theta}(t_k))]^T Q^{-1} \Lambda_\theta(\Delta t)S_\theta(\hat{\theta}(t_k)) + W_\theta\}^{-1} \\ &\times [\Lambda_\theta(\Delta t)S_\theta(\hat{\theta}(t_k))]^T Q^{-1} [Z_\theta(\hat{\theta}(t_k), \Delta t) + \hat{p}(t_k) - p(t_{k+1})] \end{aligned}$$

$$\text{Weight filter update to } \hat{\theta}(t_{k+1}) \text{ by state equation: } \dot{\hat{\theta}}(t) = r[\hat{x}(t), t, \hat{\theta}(t)] + g_\theta(t)d_\theta(t)$$

For $k=nl, 1 \leq n \leq r$, compute

$$\text{Covariance for } [d_x(t_{(k-1)l+1}), \dots, d_x(t_{kl})]: D_{x,k} = \text{Cov}[d_x(t)], \quad t \in [t_{(k-1)l+1} : t_{kl}]$$

$$\text{Covariance for } [d_\theta(t_{(k-1)l+1}), \dots, d_\theta(t_{kl})]: D_{\theta,k} = \text{Cov}[d_\theta(t)], \quad t \in [t_{(k-1)l+1} : t_{kl}]$$

$$\text{Update weighting matrix for state and weight filters: } W_x = D_{x,k}^{-1}, \quad W_\theta = D_{\theta,k}^{-1}$$

^a v, ω are independent, zero-mean, Gaussian noise processes with covariance R and Q .

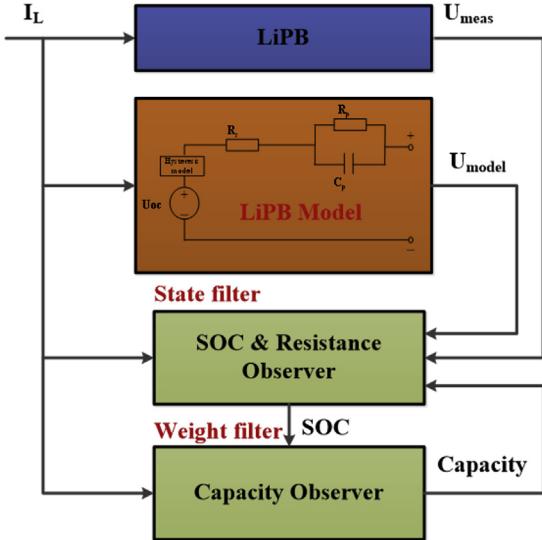


Fig. 9. Schematic diagram of DNPF for battery state estimation.

$$\text{State equation for state filter : } \dot{x}(t) = \begin{pmatrix} \dot{SOC}(t) \\ \dot{U}_p(t) \\ \dot{R}_s(t) \\ h(t) \end{pmatrix} = \begin{pmatrix} 0 \cdot SOC(t) + \frac{I_L(t)}{C} \\ -(R_p C_p)^{-1} U_p(t) + C_p^{-1} I_L(t) \\ 0 \\ -\left| \frac{\eta I_L(t) \gamma}{C} \right| h(t) + \left| \frac{\eta I_L(t) \gamma}{C} \right| M \end{pmatrix} + g_x \begin{pmatrix} d_{x,1}(t) \\ d_{x,2}(t) \\ d_{x,3}(t) \\ d_{x,4}(t) \end{pmatrix} \quad (36)$$

$$\begin{aligned} \text{Measurement equation for state filter : } y(t_k) &= U_t(t_k) \\ &= U_{oc}[SOC(t_k)] + U_p(t_k) + I_L(t_k)R_s(t_k) + h_k(t_k) + v(t_k) \end{aligned} \quad (37)$$

where the battery terminal voltage U_t is chosen as the system output variable.

In the weight filter, the capacity of the battery cell which has slow dynamic is treated as state variable, and the model for weight filter is formulated as follows:

$$\text{State equation for weight filter : } \dot{\theta}(t) = \dot{C}(t) = 0 \cdot C + g_\theta d_\theta(t) \quad (38)$$

$$\text{Measurement equation for weight filter : } p(t_k) = e(t_k)$$

$$= SOC(t_{k+1}) - SOC(t_0) + \sum_0^k \frac{\eta I_L(t_{k+1}) \Delta t}{C(t_k)} + \omega(t_k) \quad (39)$$

where the second equation is a discrete form of the SOC state equation, then the expected value of $e(t_k)$ is equal to zero. A block diagram of DNPF for battery state and parameter estimation is shown in Fig. 9.

3.4. Multi time-scale framework for pack-level estimation

Based on the previous discussion, a multi time-scale estimation framework is proposed to deal with the SOC and SOH estimation of battery pack. The proposed framework, shown in Fig. 10, extends the DNPF battery estimation methodology proposed in the previous subsection from cell-level to pack-level. The proposed framework is composed of two main parts: a long time-scale estimation part and a real-time estimation part. In the long time-scale estimation part, the DNPF is used to estimate the resistance and capacity of every in-pack cell so as to obtain the capacity and power SOH of battery pack. Meanwhile a capacity screening process is performed to select the weakest cell with minimum capacity. Compare to the battery SOC, the capacity and resistance has slower dynamic. Therefore, the estimation of capacity and resistance of every in-pack cell can be executed several weeks once which greatly reduces the computation. In the real-time SOC estimation part, a single NPF is used to estimate the pack SOC by means of estimating the SOC of the weakest cell with minimum capacity. The model parameters (e.g. resistance and capacity) used in the SOC

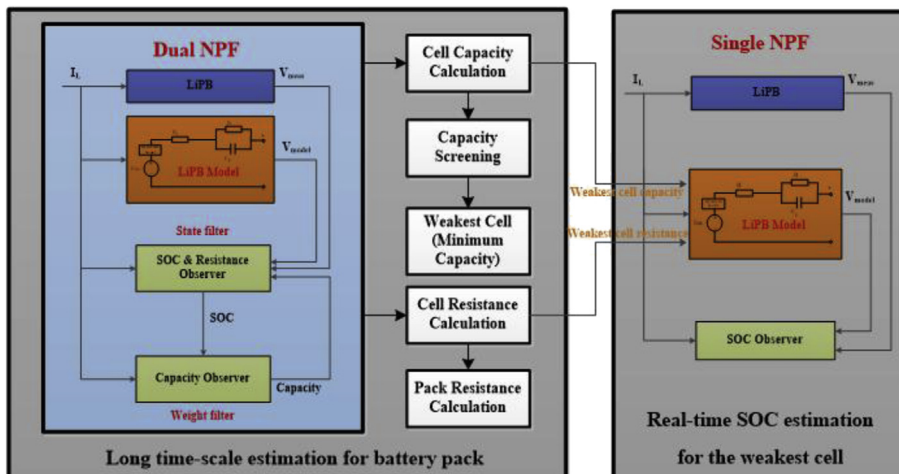


Fig. 10. Block diagram of multi time-scale framework for pack-level SOC/SOH estimation.

Table 3
LiFePO₄ battery cell specifications.

Cell dimensions(mm)	Ø 32 × 113
Cell weight(g)	205
Cell capacity (nominal, Ah)	4.5
Cell voltage (nominal, V)	3.3
Specific power (nominal, W/kg)	2700
Specific energy (nominal, Wh/kg)	71
Energy density (nominal, Wh/L)	161
Operating temperature	−30 °C to 55 °C

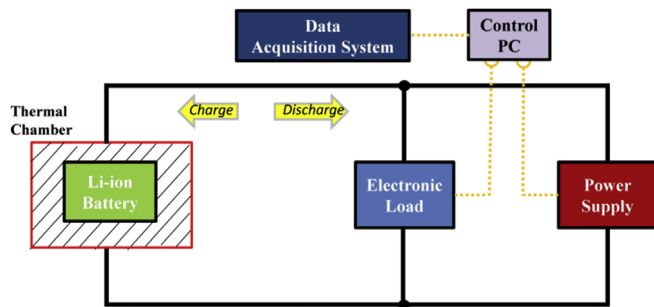


Fig. 11. Schematic of battery test bench.

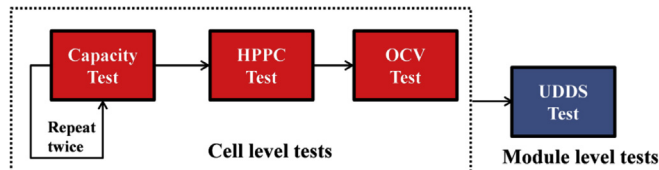


Fig. 12. Schedule of the battery tests.

estimation of the weakest cell can be updated using the previous results from the long time-scale estimation which helps increasing the model accuracy.

To realize the proposed framework in actual BMS, the long time-scale resistance and capacity estimation of each cell can be implemented with the current and voltage profiles from daily driving cycle which are stored in the memory of BMS (e.g. one day's driving profiles of EVs). Then, when the BMS is free (e.g. the EV packs at home), the estimation of every cell's capacity and resistance is executed and the screening process for the weakest cell is performed. Since the resistance and capacity of battery cell changes very slowly and can be assumed as unchanged in the short term, the long time-scale estimation with daily driving data can be implemented several weeks once. Therefore, the BMS has enough time to estimate every cell's resistance and capacity which greatly reduces the requirement of BMS's computation capability. The pack SOC is estimated in real-time using on-line current and voltage measurements, and based on the latest cell capacity screening result. The SOC estimation is conducted on the weakest cell only, which greatly reduces the computation cost.

4. Experimental validation and results

4.1. Experiment setup

To validate the propose framework, a battery pack composed of six LiFePO₄ battery cells connected in series and under passive balance control is tested. The cells are power type. Each cell has suffered from calendar and cycle aging. For the calendar aging, the

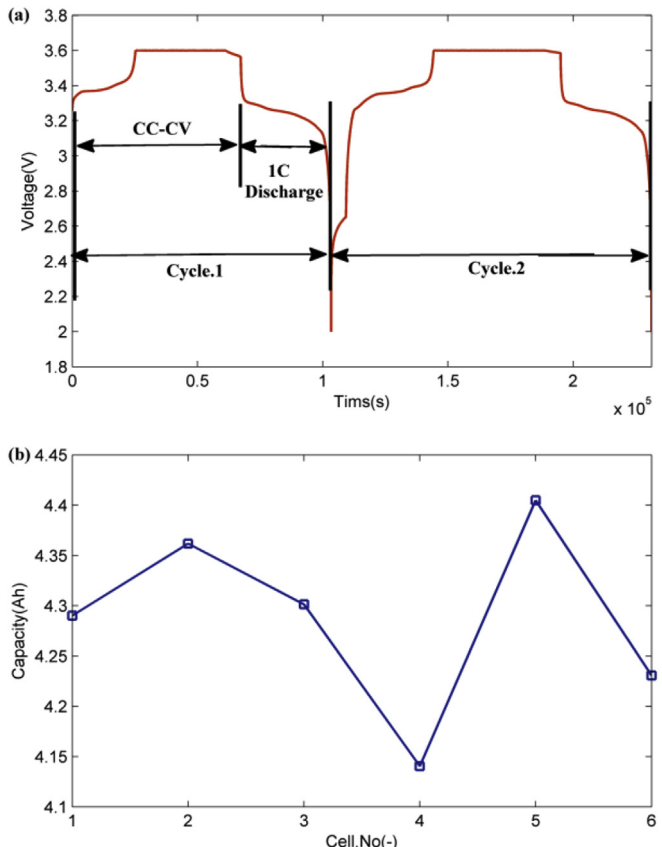


Fig. 13. Capacity tests: (a) Voltage profile of a capacity test; (b) Capacity results of the tested cells.

cells were kept stored for more than three years with different initial SOCs and under uncontrolled temperature conditions. For the cycle aging, the six cells were part of a 12-cell pack that was aged in parallel with a lead acid battery for a separate project. The cells underwent 21,000 cycles and reached about 16,500Ah throughput. The lithium batteries were passively balanced performed while the cells were charged. Therefore, the pack used in this work represents a pack that has been aged under highly imbalanced conditions and may be representative of an aged real-world EV battery pack, since nowadays the manufacturing variability of cells is very low, a fresh pack (i.e. not aged) is commonly assumed to have all the cells equal.

The nominal standard specification of the cell is listed in Table 3. The experiments were conducted in the battery characterization and aging laboratories at The Ohio State University Center for Automotive Research (OSU-CAR). The configuration of the battery test bench is shown in Fig. 11, it consisted of a pair of programmable load and power supply, a distributed data acquisition, a control computer and thermal chamber. The thermal chamber is able to provide a controlled thermal environment for battery testing with the temperatures ranging between −25 °C and +60 °C. To provide the desirable power for the tested battery cells, a computer remotely controls the programmable load and power supply. The experimental results were collected by the data acquisition system with a sampling rate of 10 Hz, and stored in the computer. All the experiments were conducted at 25 °C.

4.2. Experimental plan and battery characterization results

Fig. 12 presents a block diagram with the experimental plan. It

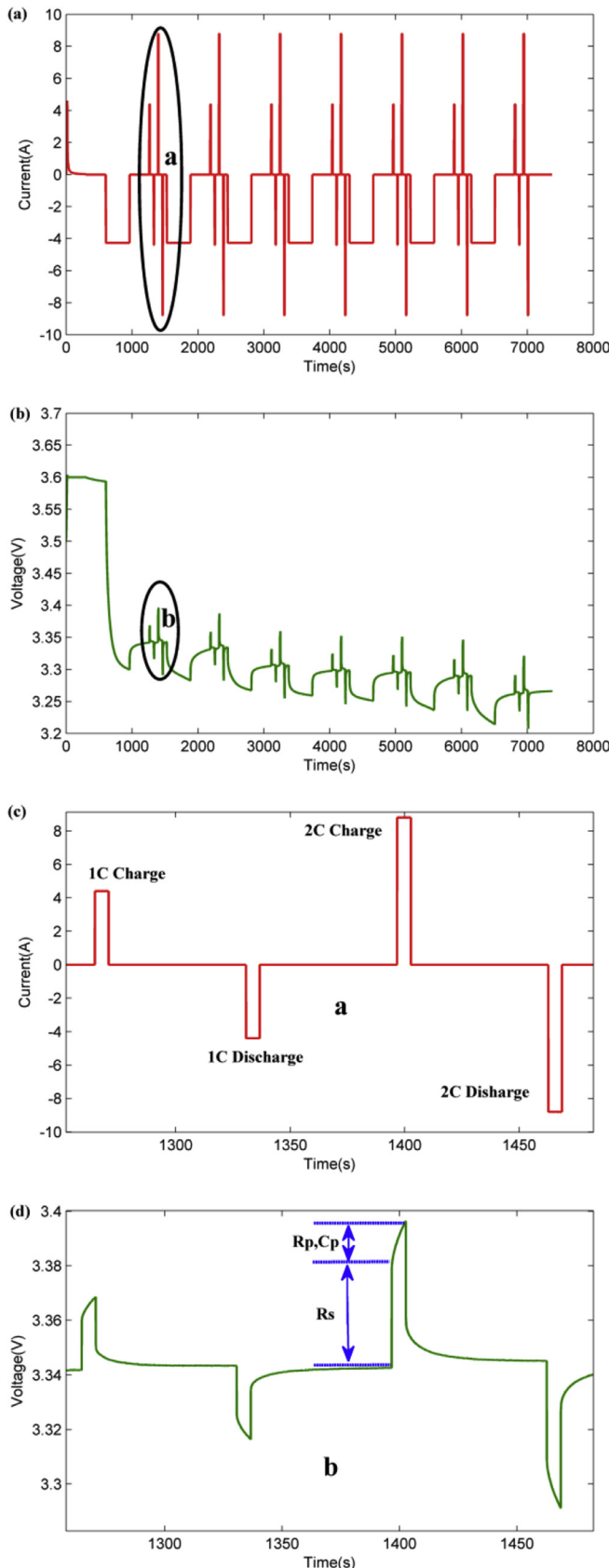


Fig. 14. HPPC test profiles: (a) Voltage profile; (b) Current profile; (c) Zoom plot of current profile; (d) Zoom plot of voltage profile.

consists of two main blocks: cell-level experiments for cells characterization and model identification; and pack-level experiments to validate the proposed estimation framework. The cell-level tests consist of capacity test, hybrid pulse power characterization (HPPC) test and open circuit voltage (OCV) test for each individual cell in the pack. The pack level UDDS test is conducted on the battery pack for the validation of proposed algorithm.

The contents of the tests are listed as follows:

- Capacity test: the battery cell is fully charged by constant-current and constant-voltage (CC-CV) charging protocol to upper-limit voltage. Then the cell is discharged using a constant current of 1C (4.5 A) to the lower-limit voltage. The voltage limits used during the test are $V_{\max} = 3.6$ V and $V_{\min} = 2$ V. The total ampere-hours drawn out of the cell from upper-limit voltage to lower-limit voltage during discharging process is indicated as the cell's nominal capacity. The test is repeated two times and the average discharging capacity is taken as the actual cell's capacity. **Fig. 13 a** shows the voltage profile during a capacity test. **Fig. 13 b** presents the capacity results for all the six individual cells.
- Hybrid pulse power characterization (HPPC) test [38]: In order to identify the parameters of the cells, HPPC test is conducted on the cells at 10% SOC interval, starting from 90% SOC and until reaching a 30% SOC. The current and voltage profiles of HPPC test are illustrated in **Fig. 14a** and **b**. The zoom plot in **Fig. 14c** And D give the current and voltage during an HPPC at 90% SOC, both charge and discharge pulses are applied with different C-rates (1C and 2C). The instantaneous voltage change when the pulse

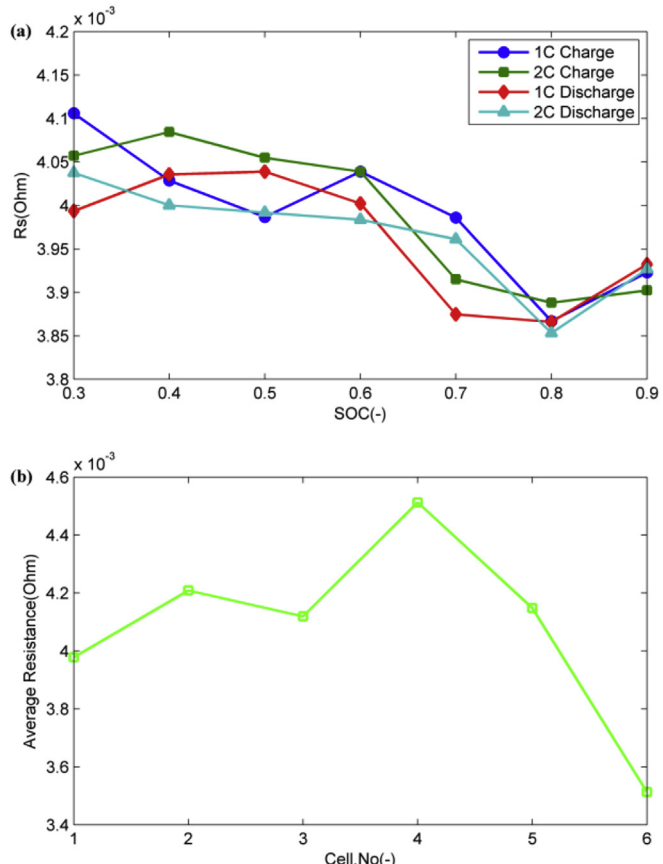


Fig. 15. Ohmic resistance identification results: (a) Resistance of cell.3 under different conditions; (b) Average resistance values for the individual cells.

charge/discharge current is applied is used for estimating the ohmic resistance R_s , while the rest dynamic part is used for estimating polarization resistance R_p and capacitance C_p . Taking cell.3 as an example, the identification results for the charge/discharge resistance under different SOCs and C-rates are given in Fig. 15a, while the average resistance values of different cells are shown in Fig. 15b. Similarly, the identification results of polarization resistance and capacitance are shown in Figs. 16 and 17.

- Open circuit voltage test: In order to calibrate the nonlinear relationship between SOC and OCV, an OCV test is conducted. For the test, the cell is firstly fully charged to upper-limit voltage using a CC-CV protocol. Then the cell is discharged by 5% of the nominal capacity and rested for 3 h to reach the close-to-equilibrium open circuit voltage. The voltage at the end of rest period is indicated as the OCV for 95% SOC. Repeatedly discharge the cell with 5% SOC interval until it is fully discharged. After each discharge interval, the cell is rested for 3 h to get the open circuit voltage at each SOC point. Similarly, charge the battery cell with an interval of 5% SOC following a similar procedure to get the open circuit voltage for charging process. According to the OCV test results, the cells in a same battery pack have similar OCV curve. As an example, the OCV curve for cell.3 is shown in Fig. 18. The experimental results show that the equilibrium potential has different values after charging and discharging, respectively, at the same SOC. The equilibrium potential is lower at the discharging process than that at the charging process. The difference of the equilibrium potential after charging and

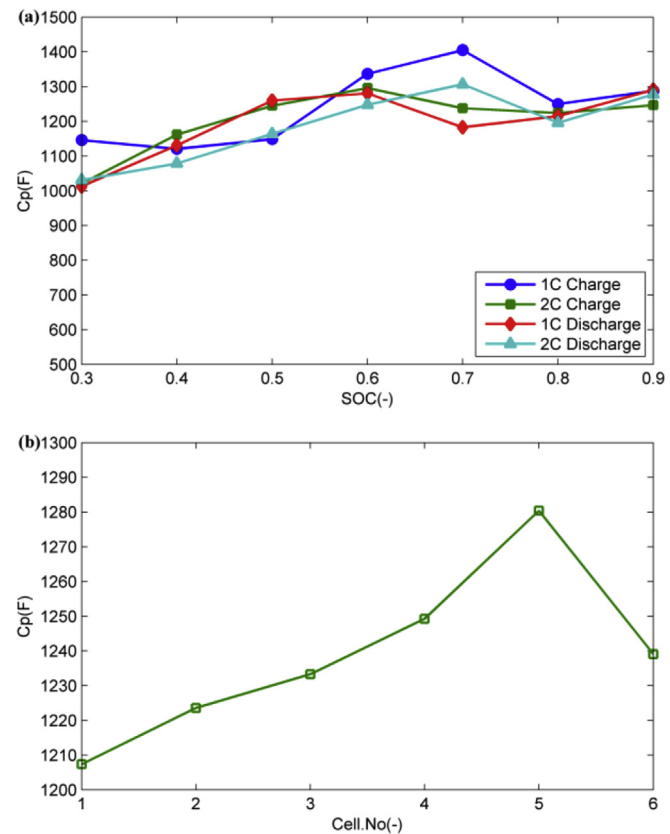


Fig. 17. Polarization capacitance identification results: (a) Polarization capacitance of cell.3 under different conditions; (b) Average polarization capacitance values for the individual cells.

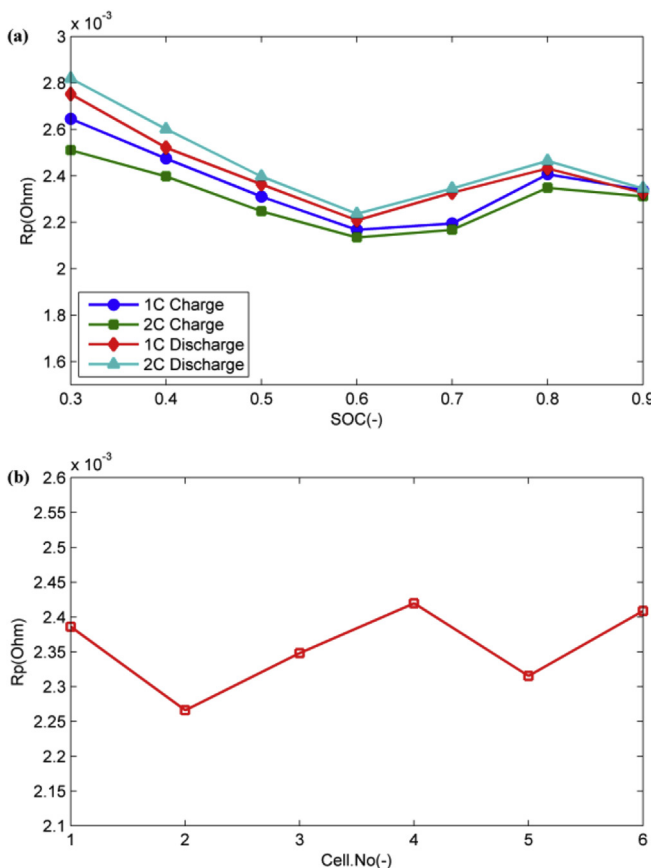


Fig. 16. Polarization resistance identification results: (a) Polarization resistance of cell.3 under different conditions; (b) Average polarization resistance values for the individual cells.

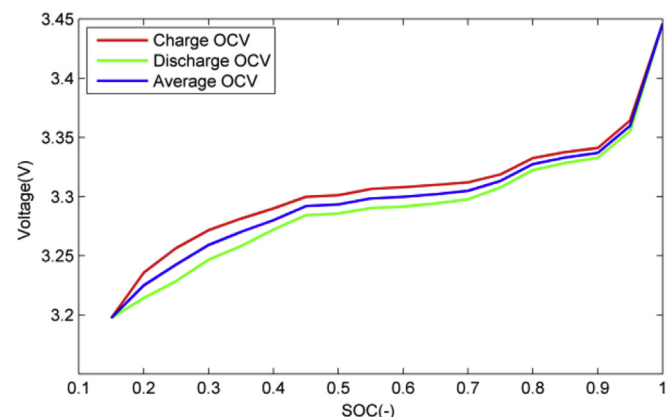


Fig. 18. Open circuit voltage curves for cell.3.

discharging process is described by the hysteresis voltage in the battery model.

- UDDS driving cycle test: UDDS stands for Urban Dynamometer Driving Schedule [39], this test is designed to simulate the battery pack dynamics under a realistic daily EV scenario. To translate the UDDS cycle, which is a velocity profile, into a current profile for the battery cell/pack, a Simulink simulator of a generic EV was used. The obtained current profile was then used as input profile for the cell/pack level experiments. A typical current profile of a UDDS driving cycle is shown in Fig. 19a And B and its corresponding battery cell voltage

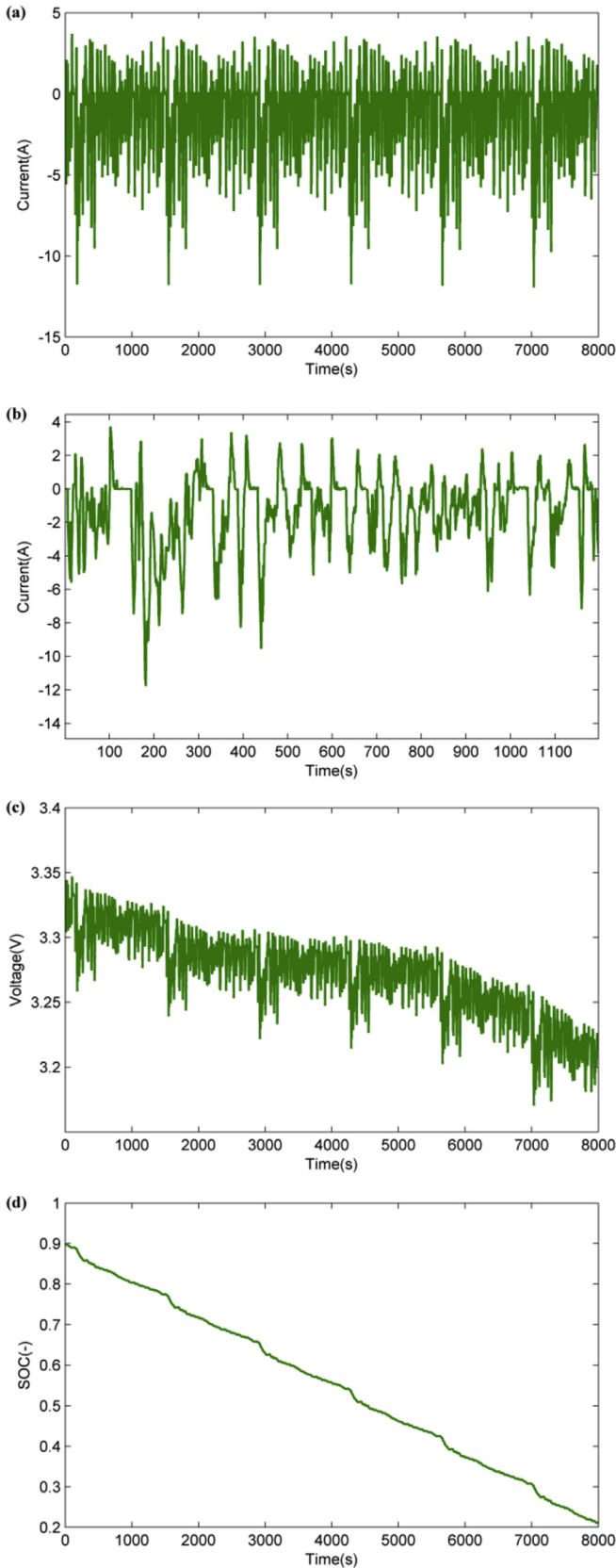


Fig. 19. UDDS profiles: (a) Current profile; (b) Zoom plot of current profile; (c) Voltage profile; (d) SOC profile.

response is shown in Fig. 19 c. To follow the practical daily driving condition of EVs, the start SOC is set as 90% to prevent the battery cell from over-charge, and the UDDS driving cycle ends with the SOC around 20% to prevent the battery cell from over-discharge (see Fig. 19d) [18]. For the pack-level test, the UDDS loading profile is applied to battery pack composed of six battery cells connected in series, each cell was provided with a voltage sensor to collect the individual cell's terminal voltage. Before the UDDS driving cycle test, the SOC of the cells were balanced to 90% SOC to ensure the cells have same initial states. The result of UDDS test is used for evaluating the performance of the proposed algorithms.

4.3. Cell-level estimation results

In this section, the accuracy of cell-level DNPF estimation approach is evaluated using the UDDS load profile which simulates the daily driving profiles of EVs. As an example, we use the results of cell.3 to analyze the estimation performance of the proposed algorithm (Similar results are obtained for the other cells). The initial states and parameters used in DNPF are listed in Table 4. To simplify the estimation algorithm and reduce the computation, the average model parameters are used in the battery model for estimation purpose, and the hysteresis voltage magnitude M is assumed to be a constant value (positive for charge and negative for discharge). In addition, the estimation time step for DNPF is set as 0.1s.

The SOC estimation results for cell.3 with accurate initial values are shown in Fig. 20. Fig. 20a shows the comparative profiles of estimated SOC and reference SOC, while Fig. 20b gives the estimation error which is less than 3%. It can be seen that the error of SOC estimation is larger in the middle SOC range than that in other SOC ranges, a zoom plot for comparative profiles of estimated SOC and reference SOC in middle SOC range is shown in Fig. 20c. Fig. 20d shows the SOC-OCV curve used in battery model, the SOC-OCV curve is quite flat in the middle SOC range which means that observability of the model-based estimation is poor in middle SOC and thus has lower estimation accuracy.

To study the robustness of the proposed algorithm to different initial SOCs, a simulation analysis is conducted. Two different initial SOC values with +10% offset and -30% offset to the true value are preset in the estimation algorithm. The comparative profiles of SOC estimation with different initial SOCs are shown in Fig. 21a, while the profiles of the estimation errors are shown in Fig. 21b. The analysis shows that the proposed algorithm is robust to different initial values and the SOC estimation can quickly converge to the true solution with several sampling intervals.

The resistance estimation results of cell.3 are shown in Fig. 22.

Table 4
Initial values and model parameters used in DNPF.

Initial states	
Initial SOC (–)	0.9
Initial resistance R_s (ohm)	4.12×10^{-3}
Initial capacity C (Ah)	4.31
Initial polarization voltage U_p (V)	0
Initial hysteresis voltage h (V)	0
Initial weighting matrices W_x, W_θ	$I_{4 \times 4}, 1$
Model parameters	
Polarization resistance R_p (ohm)	2.35×10^{-3}
Polarization capacitance C_p (F)	1233
Hysteresis transition factor γ (–)	50
Hysteresis voltage magnitude M (V)	0.015
Coulombic efficiency η (–)	1
Model error distribution matrix g_x, g_θ	$I_{4 \times 4}, 1$

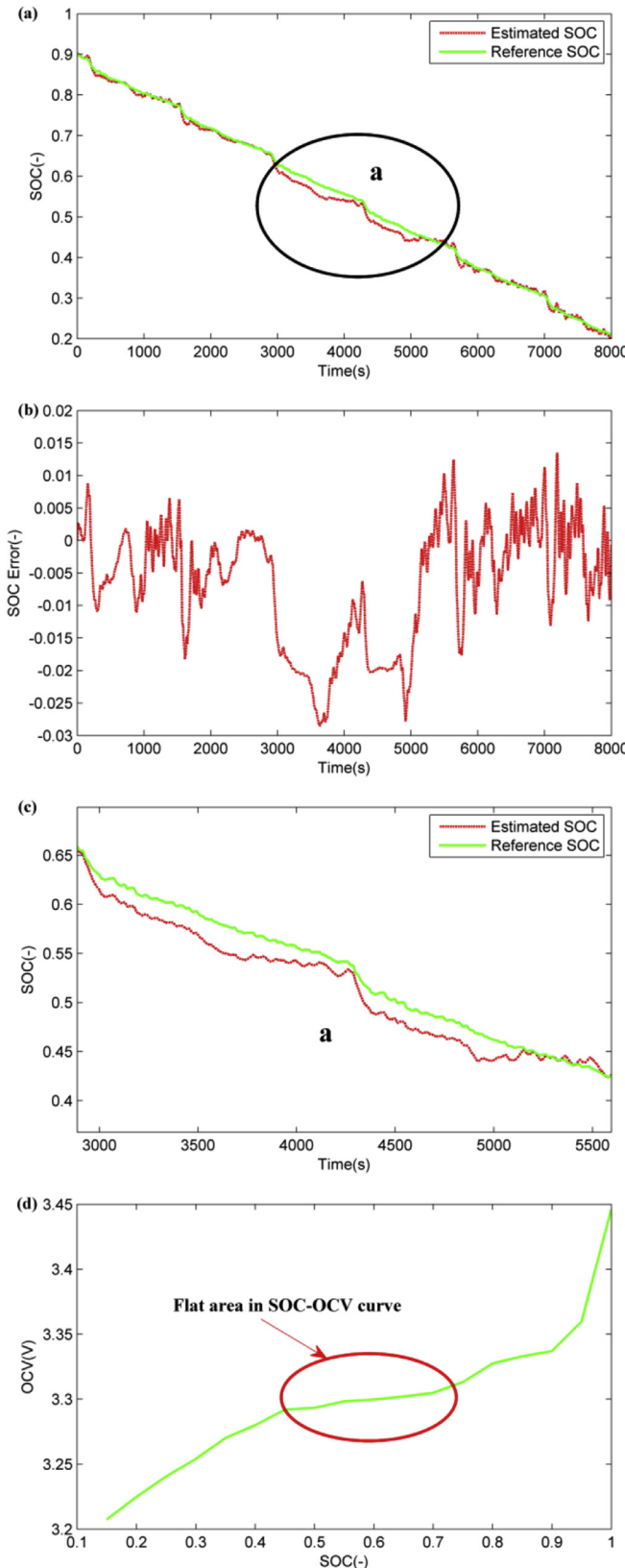


Fig. 20. SOC estimation results of cell.3: (a) SOC estimation; (b) Error of SOC estimation; (c) Zoom plot in SOC estimation; (d) SOC-OCV curve.

Fig. 22a shows the comparative profiles of the estimated resistance and reference resistance with accurate initial resistance. The corresponding estimation error is shown in **Fig. 22b**, it can be seen that the maximum error is around 4%, and the resistance estimation result has some variation within the estimation time length since the dynamic UDDS loading profiles is applied. According to the definition in Section.2, the resistance is used to calculate the power SOH of battery cell; it may lower the passengers' satisfaction if the varied power SOH is displayed onboard. Therefore, in order to obtain a stable estimation result, the average resistance is used to indicate the resistance of corresponding cell. **Fig. 22c** shows the resistance estimation results under different initial values, while **Fig. 22d** gives the corresponding errors, it can be seen that the proposed algorithm can accurately estimate the battery resistance with inaccurate initial values, the estimation is able to converge to the true solution within certain sampling intervals.

The capacity estimation result using the proposed DNPF approach with accurate initial capacity is shown in **Fig. 23a**, while **Fig. 23b** shows the relative error of capacity estimation. As illustrated in the figure, the analysis of capacity estimation can be divided into three regions. The first one, region.a, is the estimation convergence region where the capacity estimation tries to converge to the true value. Within this region, the estimation result suffers from large fluctuations since the estimating time is not long enough to get accurate capacity estimate. The capacity estimation in region.b is under middle SOC range, as previously described, the SOC estimation result under the middle SOC range has a lower accuracy due to the flat SOC-OCV curve. Therefore, the capacity estimation also suffers from large error since the estimated SOC is part of the inputs when estimating the capacity by DNPF. In regions.c, accurate capacity estimation result is obtained. However,

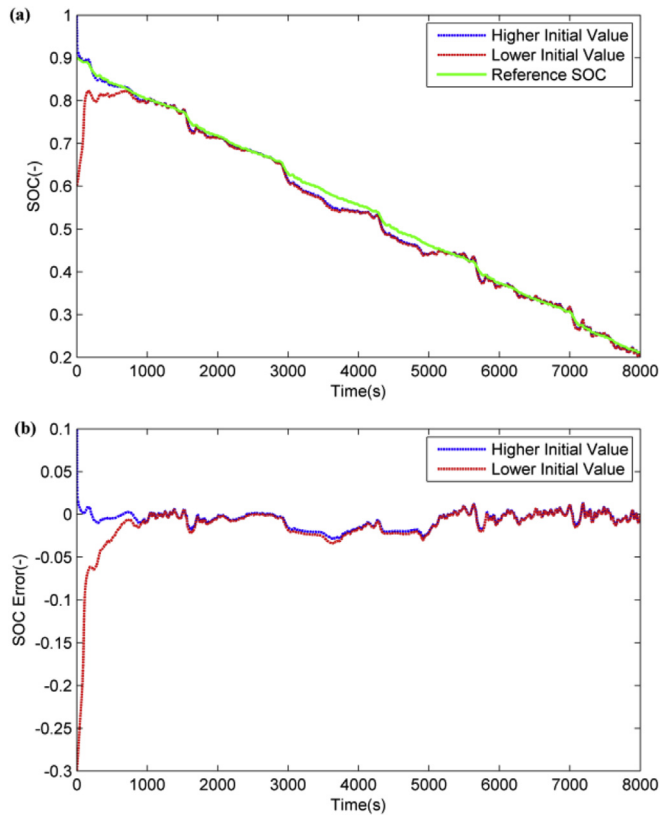


Fig. 21. SOC estimation with different initial values: (a) SOC estimation; (b) Error of SOC estimation.

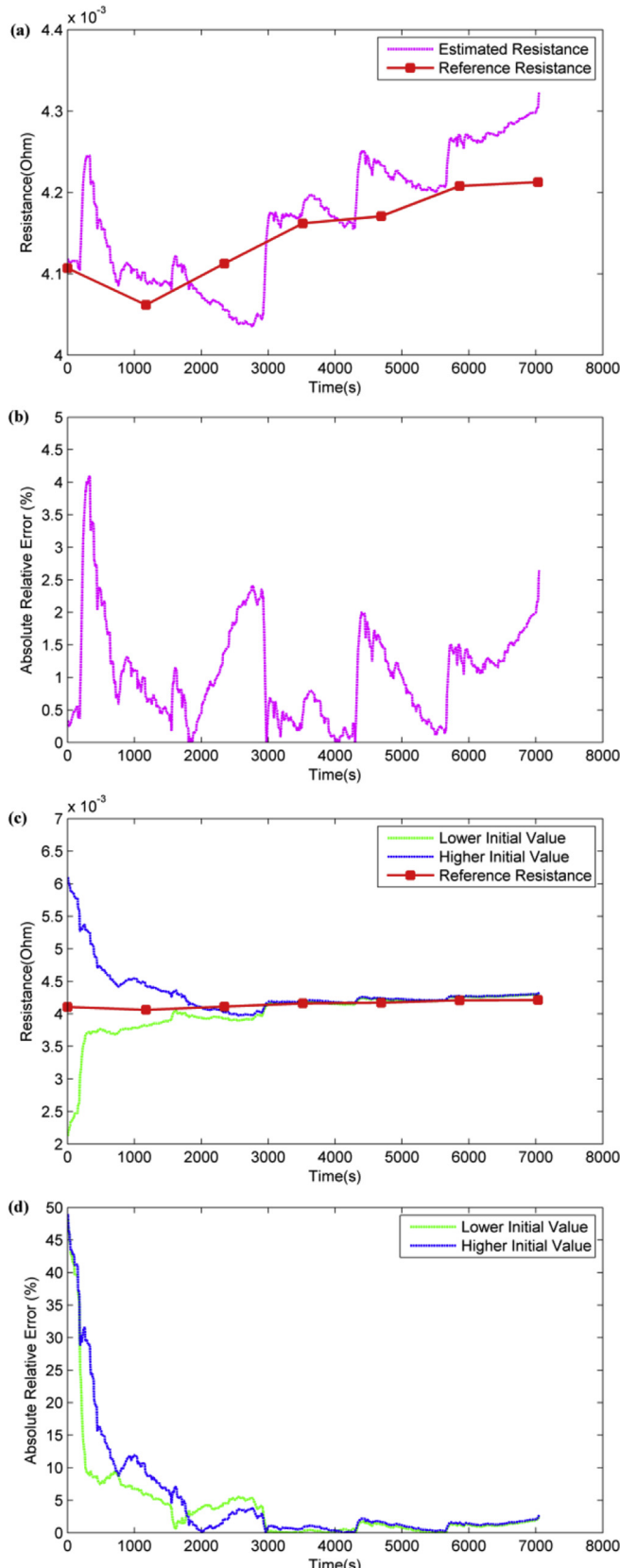


Fig. 22. Resistance estimation results of cell.3: (a) Resistance estimation; (b) Error of resistance estimation; (c) Resistance estimation with different initial values; (d) Error of resistance estimation with different initial values.

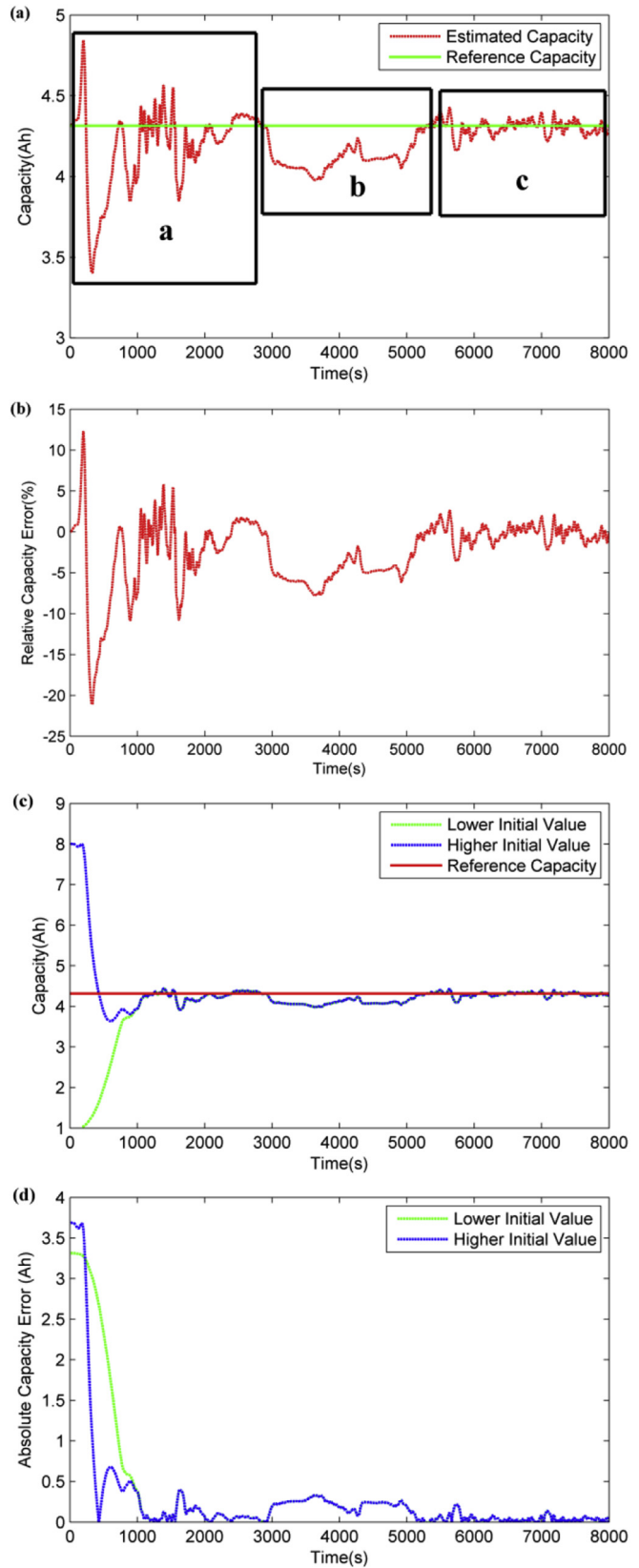


Fig. 23. Capacity estimation results of cell.3: (a) Capacity estimation; (b) Relative error of capacity estimation; (c) Capacity estimation with different initial values; (d) Absolute error of capacity estimation with different initial values.

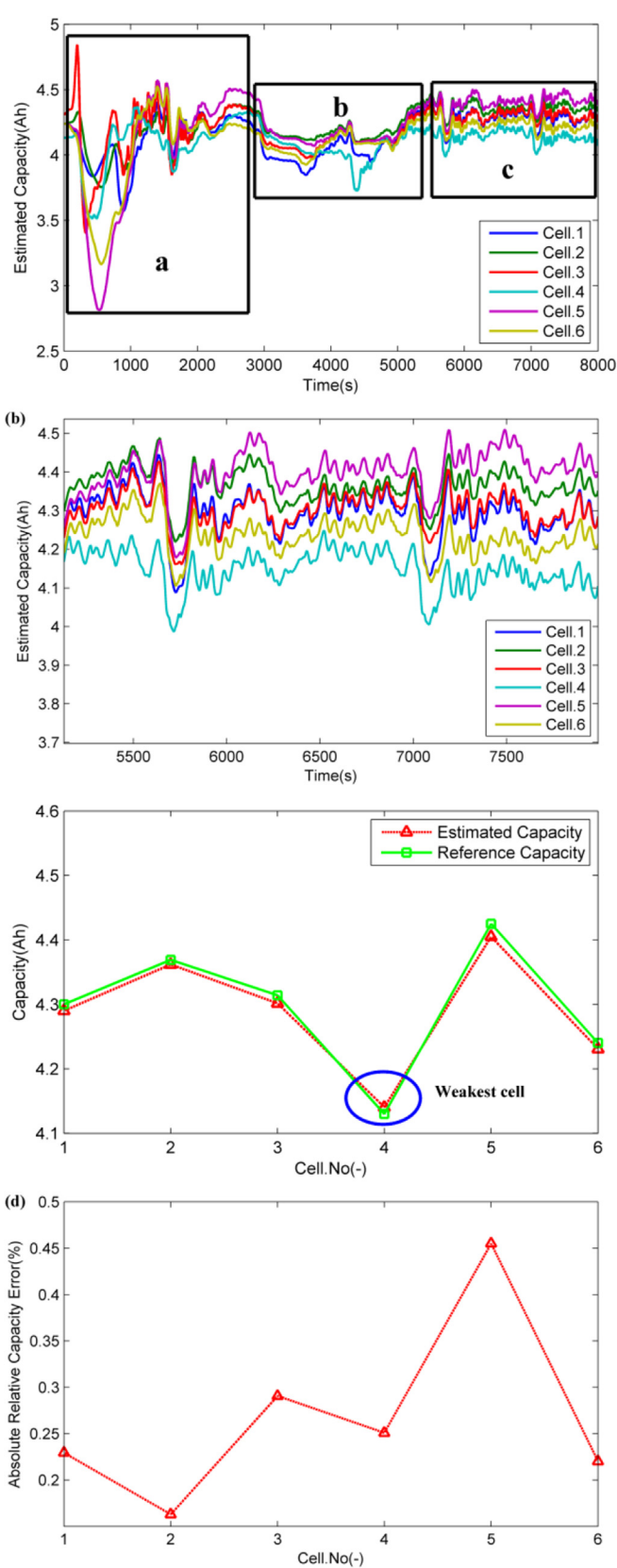


Fig. 24. Capacity estimation results with long time-scale: (a) Capacity estimation results of the cells; (b) Zoom plot of capacity estimation in region.c; (c) Comparison of capacity results; (d) Errors of estimated capacities.

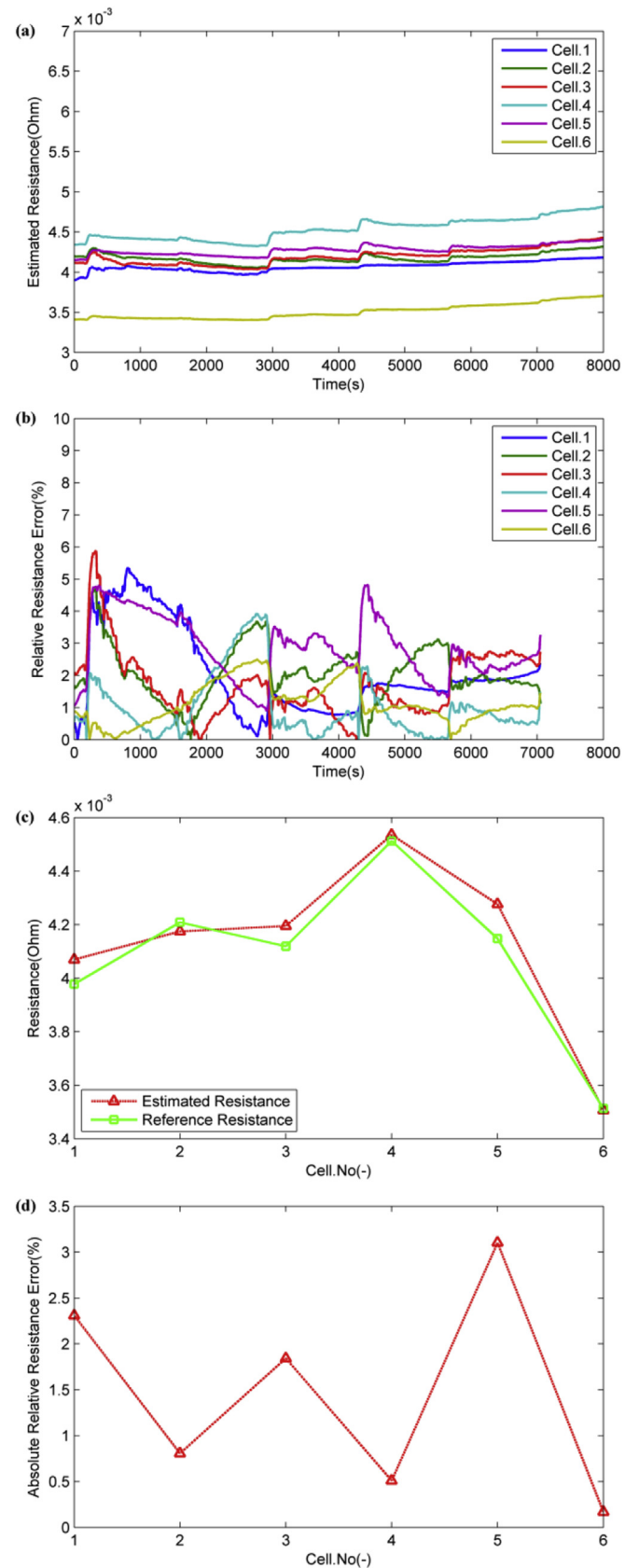


Fig. 25. Resistance estimation results with long time-scale: (a) Resistance estimation results of the cells; (b) Error of the resistance estimation; (c) Comparison of average resistance results; (d) Errors of estimated average resistances.

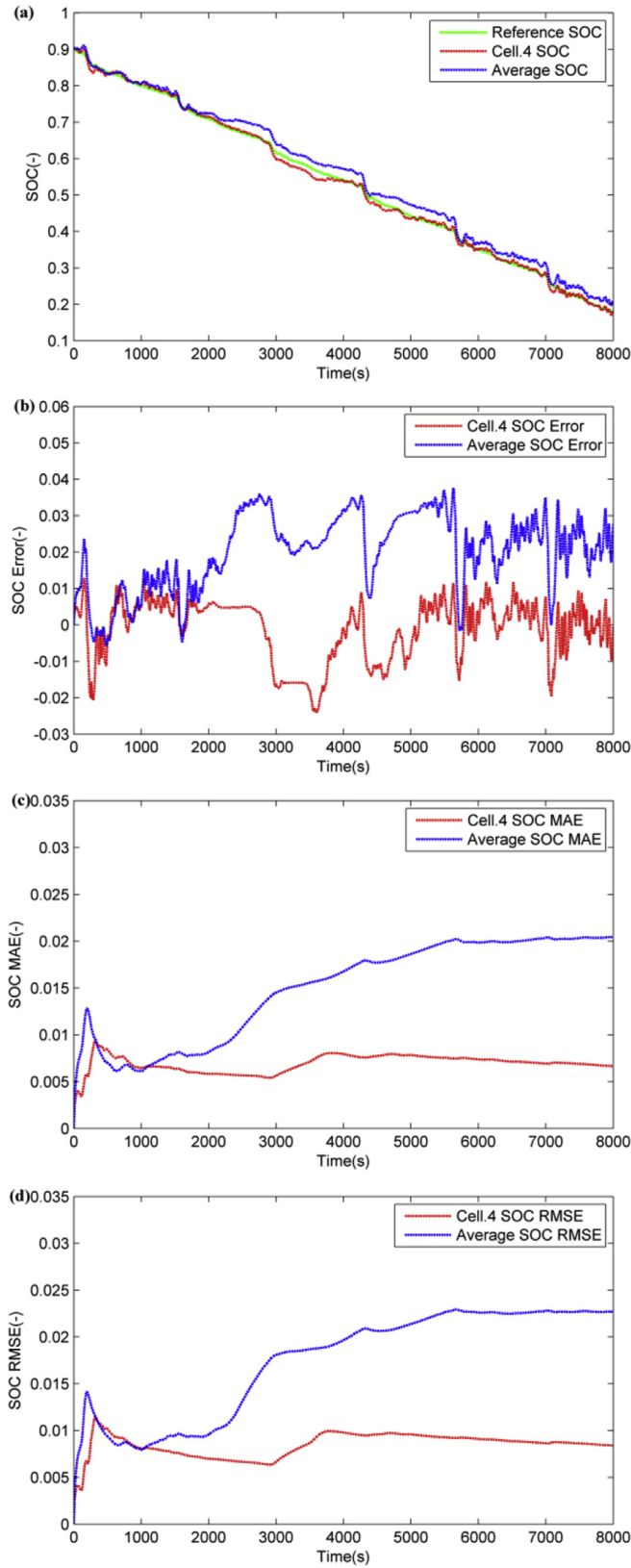


Fig. 26. Real-time SOC estimation results: (a) Comparison results of SOC estimation; (b) Error of the SOC estimation; (c) MAE of SOC estimation; (d) RMSE of SOC estimation.

the estimated capacity in region.c still has some small variation, in order to obtain a stable capacity value; the average value is calculated based on the capacity estimation results of region.c to indicate the capacity of the cell. To evaluate the robustness performance of capacity estimation, different initial capacities are applied. The comparative profiles of capacity estimation with different initial values are shown in Fig. 23c, while Fig. 23d gives the corresponding errors. It can be seen that the capacity estimation can quickly converge to the true solution with several sampling intervals.

4.4. Pack-level estimation results

In this section, the pack-level estimation using the proposed multi time-scale estimation framework is evaluated. The UDDS loading profile is applied to battery pack composed of six battery cells connected in series, each cell is provided with a voltage sensor to collect the individual cell's terminal voltage. Before the UDDS driving cycle test, the SOC of the cells were balanced to 90% SOC to ensure the cells have same initial states. The capacity and resistance estimation results of the cells within the pack under UDDS loading profiles are shown in Figs. 24 and 25. Fig. 26 shows the SOC estimation results for the battery pack under UDDS loading profiles.

Fig. 24a shows the estimated capacities of six cells, while Fig. 24b gives the zoom plot of capacity estimation results in region.c. As described in Section 4.3, the final capacity values of the cells are calculated based on the average value of the estimated capacities in region.c, Fig. 24c shows the comparative results of estimated capacities and reference capacities for different cells and Fig. 24d gives the absolute relative capacity errors of the cells, it can be found that cell.5 has the maximum estimation error which is around 0.45%. According to the results, the weakest cell (cell.4) with minimum capacity can be screened, and then the capacity of the battery pack is equal to the averaged capacity of cell.4 which can be further used to obtain the capacity SOH of battery pack according to the definition in Eq. (9).

Fig. 25a shows the resistance estimation results of the six cells, while Fig. 25b gives the estimation errors, it can be seen that the maximum error of the estimated resistances is less than 6%. Fig. 25c shows the comparative results of average resistances and reference resistances for different cells, and Fig. 25d gives the absolute relative resistance errors of the cells. It can be seen that cell.5 has the maximum error which is around 3%. According to the results, the cell with largest resistance (cell.4) can be obtained, and then the pack power SOH can be determined by the resistance of cell.4 based on the definition in Eq. (10).

The SOC estimation results are shown in Fig. 26. Here, a comparison study for SOC estimation of battery pack is conducted between the proposed algorithm and with a commonly applied estimation approach. A common approach to estimate the pack SOC is implemented using a unit battery model, where the parameters for the unit model are adopted as the average values of all the cells within the same pack. For convenience, the estimated SOC with unit model is indicated as 'average SOC' here. For the proposed algorithm, the pack SOC is equal to the SOC of the weakest cell with minimum capacity, which is cell.4 due to previous capacity screening result. The comparison results of 'average SOC' and cell.4 SOC are shown in Fig. 26a, while Fig. 26b gives the corresponding estimation errors. It can be seen that the maximum estimation error using unit model is around 4%, and it is larger than the maximum estimation error of the proposed algorithm, which is around 2%. Fig. 26c and d shows the mean absolute error (MAE) and root mean squared error (RMSE) of SOC estimation by these two algorithms, the proposed algorithm also shows a better accuracy according to the MAE and RMSE results.

5. Conclusions

In this work, a multi time-scale estimation framework is proposed to estimate the states of battery pack. The SOC and SOH definitions are extended from cell-level to pack-level for a series connected battery pack with passive balance control. A multi time-scale estimation framework is developed. The proposed framework separates the estimation of pack states into two different time scales: long time-scale and real-time estimation. In long time-scale estimation part, DNPF is applied to estimate the capacity and resistance of every single cell in order to obtain the capacity and power SOH of the battery pack. A capacity screening process is then performed to obtain the weakest cell with minimum capacity among the in-pack cells. In real-time estimation part, the SOC of the weakest cell which represents the SOC of pack is estimated online by a single NPF. Finally, the experimental validation using UDDS driving cycle is applied. The validation results for long time-scale estimation show that the proposed algorithm is able to accurately estimate the resistance and capacity of every in-pack cell. The validation results of SOC estimation indicate that the proposed algorithm has better estimation accuracy than the SOC estimation based on unit cell model. The current work mainly focuses on the SOC and SOH estimation for an aged battery pack based on dynamic load; the future work will mainly focus on the validation of the proposed framework in a long term (e.g. hundreds of cycles or months of storage) and use the SOH estimation results for diagnosis of the remaining useful life (RUL) of battery pack.

Disclaimer

Any opinions, findings, and conclusions or recommendations expressed in this material are those of the author(s) and do not necessarily reflect the views of the National Science Foundation.

Acknowledgments

The authors wish to thank Prof. Wei Zhang as well as Yilu Zhang and Xindu Du from General Motors for their invaluable contributions. This material is based upon work supported by the National Science Foundation under Grant Number NSF-1301238.

References

- [1] K. Striebel, J. Shim, A. Sierra, et al., The development of low cost LiFePO₄ based high power lithium-ion batteries, *J. Power Sources* 146 (1) (2005) 33–38.
- [2] S.M. Lukic, J. Cao, R.C. Bansal, et al., Energy storage systems for automotive applications, *Industrial Electron. IEEE Trans.* 55 (6) (2008) 2258–2267.
- [3] K.S. Ng, C.S. Moo, Y.P. Chen, et al., Enhanced coulomb counting method for estimating state-of-charge and state-of-health of lithium-ion batteries, *Appl. Energy* 86 (9) (2009) 1506–1511.
- [4] J. Garche, A. Jossen, H. Döring, The influence of different operating conditions, especially over-discharge, on the lifetime and performance of lead/acid batteries for photovoltaic systems, *J. Power Sources* 67 (1) (1997) 201–212.
- [5] J. Remmlinger, M. Buchholz, M. Meiler, et al., State-of-health monitoring of lithium-ion batteries in electric vehicles by on-board internal resistance estimation, *J. Power Sources* 196 (12) (2011) 5357–5363.
- [6] C. Hu, B.D. Youn, J. Chung, A multiscale framework with extended Kalman filter for lithium-ion battery SOC and capacity estimation, *Appl. Energy* 92 (2012) 694–704.
- [7] Y. Zheng, X. Han, L. Lu, et al., Lithium ion battery pack power fade fault identification based on Shannon entropy in electric vehicles, *J. Power Sources* 223 (2013) 136–146.
- [8] V.H. Johnson, Battery performance models in ADVISOR, *J. Power Sources* 110 (2) (2002) 321–329.
- [9] S. Piller, M. Perrin, A. Jossen, Methods for state-of-charge determination and their applications, *J. Power Sources* 96 (1) (2001) 113–120.
- [10] Y. Xing, W. He, M. Pecht, et al., State of charge estimation of lithium-ion batteries using the open-circuit voltage at various ambient temperatures, *Appl. Energy* 113 (2014) 106–115.
- [11] I. Snihir, W. Rey, E. Verbitskiy, et al., Battery open-circuit voltage estimation by a method of statistical analysis, *J. Power Sources* 159 (2) (2006) 1484–1487.
- [12] C.C. Chan, E.W.C. Lo, S. Weixiang, The available capacity computation model based on artificial neural network for lead-acid batteries in electric vehicles, *J. Power Sources* 87 (1) (2000) 201–204.
- [13] T. Hansen, C.J. Wang, Support vector based battery state of charge estimator, *J. Power Sources* 141 (2) (2005) 351–358.
- [14] I.S. Kim, The novel state of charge estimation method for lithium battery using sliding mode observer, *J. Power Sources* 163 (1) (2006) 584–590.
- [15] G.L. Plett, Extended Kalman filtering for battery management systems of LiPB-based HEV battery packs: part 3. State and parameter estimation, *J. Power Sources* 134 (2) (2004) 277–292.
- [16] G.L. Plett, Sigma-point Kalman filtering for battery management systems of LiPB-based HEV battery packs: part 2: simultaneous state and parameter estimation, *J. Power Sources* 161 (2) (2006) 1369–1384.
- [17] J. Han, D. Kim, M. Sunwoo, State-of-charge estimation of lead-acid batteries using an adaptive extended Kalman filter, *J. Power Sources* 188 (2) (2009) 606–612.
- [18] F. Sun, X. Hu, Y. Zou, et al., Adaptive unscented Kalman filtering for state of charge estimation of a lithium-ion battery for electric vehicles, *Energy* 36 (5) (2011) 3531–3540.
- [19] Y. He, X.T. Liu, C.B. Zhang, et al., A new model for state-of-charge (SOC) estimation for high-power Li-ion batteries, *Appl. Energy* 101 (2013) 808–814.
- [20] I.S. Kim, A technique for estimating the state of health of lithium batteries through a dual-sliding-mode observer, *Power Electron. IEEE Trans.* 25 (4) (2010) 1013–1022.
- [21] B. Kenney, K. Darovich, D.D. MacNeil, et al., Modelling the impact of variations in electrode manufacturing on lithium-ion battery modules, *J. Power Sources* 213 (2012) 391–401.
- [22] M. Dubarry, C. Truchot, M. Cugnet, et al., Evaluation of commercial lithium-ion cells based on composite positive electrode for plug-in hybrid electric vehicle applications. Part I: initial characterizations, *J. Power Sources* 196 (23) (2011) 10328–10335.
- [23] G.L. Plett, Efficient Battery Pack State Estimation Using Bar-delta Filtering, *EVS24 Stavanger*, 2009, pp. 13–16.
- [24] H. Dai, X. Wei, Z. Sun, et al., Online cell SOC estimation of Li-ion battery packs using a dual time-scale Kalman filtering for EV applications, *Appl. Energy* 95 (2012) 227–237.
- [25] J. Kim, J. Shin, C. Chun, et al., Stable configuration of a Li-ion series battery pack based on a screening process for improved voltage/SOC balancing, *Power Electron. IEEE Trans.* 27 (1) (2012) 411–424.
- [26] R. Xiong, F. Sun, X. Gong, et al., Adaptive state of charge estimator for lithium-ion cells series battery pack in electric vehicles, *J. Power Sources* 242 (2013) 699–713.
- [27] M.A. Roscher, O.S. Bohlen, D.U. Sauer, Reliable state estimation of multicell lithium-ion battery systems, *Energy Convers. IEEE Trans.* 26 (3) (2011) 737–743.
- [28] Y. Zheng, M. Ouyang, L. Lu, et al., Cell state-of-charge inconsistency estimation for LiFePO₄ battery pack in hybrid electric vehicles using mean-difference model, *Appl. Energy* 111 (2013) 571–580.
- [29] L. Zhong, C. Zhang, Y. He, et al., A method for the estimation of the battery pack state of charge based on in-pack cells uniformity analysis, *Appl. Energy* 113 (2014) 558–564.
- [30] X. Liu, Y. He, Z. Chen, State-of-charge estimation for power Li-ion battery pack using Vmin-EKF, in: Second International Conference on Software Engineering and Data Mining (SEDM), 2010, pp. 27–31.
- [31] J.L. Crassidis, F.L. Markley, Predictive filtering for attitude estimation without rate sensors, *J. Guid. Control Dyn.* 20 (3) (1997) 522–527.
- [32] A. Cordoba-Arenas, S. Onori, G. Rizzoni, A control-oriented lithium-ion battery pack model for plug-in hybrid electric vehicle cycle-life studies and system design with consideration of health management, *J. Power Sources* 279 (2015) 791–808.
- [33] S.W. Moore, P.J. Schneider, A Review of Cell Equalization Methods for Lithium Ion and Lithium Polymer Battery Systems, SAE Technical Paper, 2001.
- [34] Y. Zheng, L. Lu, X. Han, et al., LiFePO₄ battery pack capacity estimation for electric vehicles based on charging cell voltage curve transformation, *J. Power Sources* 226 (2013) 33–41.
- [35] J. Marcicki, M. Canova, A.T. Conlisk, et al., Design and parametrization analysis of a reduced-order electrochemical model of graphite/LiFePO₄ cells for SOC/SOH estimation, *J. Power Sources* 237 (2013) 310–324.
- [36] X. Hu, S. Li, H. Peng, A comparative study of equivalent circuit models for Li-ion batteries, *J. Power Sources* 198 (2012) 359–367.
- [37] D.J. Mook, J.L. Junkins, Minimum model error estimation for poorly modeled dynamic systems, *J. Guid. Control, Dyn.* 11 (3) (1988) 256–261.
- [38] United States Department of Energy, Vehicle Technology Program, Electric Vehicle Battery Test Procedures Manual, Revision 3, September 2014.
- [39] US Environmental Protection Agency, EPA urban dynamometer driving schedule (UDDS). <http://www.epa.gov/oms/standards/light-duty/udds.htm>.
- [40] J. Vetter, P. Novak, M.R. Wagner, et al., Ageing mechanisms in lithium-ion batteries, *J. Power Sources* 147 (1) (2005) 269–281.
- [41] S. Onori, P. Spagnol, V. Marano, et al., A new life estimation method for lithium-ion batteries in plug-in hybrid electric vehicles applications, *Int. J. Power Electron.* 4 (3) (2012) 302–319.

- [42] K. Goebel, B. Saha, A. Saxena, et al., Prognostics in battery health management, *IEEE Instrum. Meas. Mag.* 11 (4) (2008) 33.
- [43] J. Remmlinger, M. Buchholz, M. Meiler, et al., State-of-health monitoring of lithium-ion batteries in electric vehicles by on-board internal resistance estimation, *J. Power Sources* 196 (12) (2011) 5357–5363.
- [44] D. Andre, C. Appel, T. Soczka-Guth, et al., Advanced mathematical methods of SOC and SOH estimation for lithium-ion batteries, *J. Power Sources* 224 (2013) 20–27.
- [45] D. Haifeng, W. Xuezhe, S. Zechang, A new SOH prediction concept for the power lithium-ion battery used on HEVs, in: *Vehicle Power and Propulsion Conference, 2009. VPPC'09. IEEE, IEEE, 2009*, pp. 1649–1653.